Turnitin Statement:

The relative similarity score obtained was 21%, to 144 documents, with no more than 1% similarity to any specific document.

The primary similarities were as follows: The electronic declaration, extended gene names, long-form chemical names such as ‘4-Methylumbelliferyl N-sulpho-α-D-glucosaminide’, technical phrases such as ‘catalyses the cleavage of sulfate groups from heparan sulfate’ or ‘Statistical analysis performed via one-way ANOVA with Bonferroni post-hoc testing in GraphPad Prism.’, and the reference list.

Overall, the similarity score and specific similarities did not indicate any need for changes.

Evaluation of a nanoparticle-based gene therapy vector for treatment of Sanfilippo syndrome.

Submission by

William Scott

Supervisors

Professor Kim Hemsley and Dr Adeline Lau

Flinders University

College of Medicine and Public Health

Submitted 9th of May 2023

Table of Contents:

Abstract

Mucopolysaccharidosis (MPS) IIIA, or Sanfilippo syndrome, is a lysosomal storage disorder of the mucopolysaccharidosis family, where a mutated *N*-sulfoglucosamine sulfohydrolase (*SGSH*) gene results in impaired production or function of the sulfamidase enzyme. This enzyme normally plays a critical role in the degradation of heparan sulfate, a long-chain glycosaminoglycan. As a result of this enzyme deficiency, heparan sulfate builds up in body tissues and causes a range of issues with an early onset of 2-4 years of age, most notably progressive and severe neurological impairment that eventually requires full-time care and leads to death by the late teens to early twenties.

Currently, no treatment exists for Sanfilippo syndrome, although multiple therapeutic approaches are being investigated. Importantly, removal of the accumulated excess heparan sulfate does not correct accumulated damage, so treatment must be started from an early age. One of the most promising avenues is gene therapy, where plasmids containing wildtype *SGSH* genes are delivered into cells via a vector to then express the required enzyme continuously in the body. Such therapies could provide a long-lasting treatment effect, although they would need to be repeated every few years as the number of cells in the patient's body multiplies. Unfortunately, the currently used viral vectors face major issues with immunogenicity and pre-existing antibodies. This means that viral vectors are not suitable for a large portion of patients, and each successive treatment for a given patient will be less effective, rendering the approach unable to provide the repeated treatments needed over a patient's lifetime.

Lipid nanoparticles are an emerging area of research that have the potential to provide alternative, non-immunogenic vector. Prior studies showed that a specific liposome formulation effectively induced expression of a green fluorescent protein in cell and mouse models. This project hypothesized that the nanoparticles would also effectively deliver the *SGSH* gene and effectively induce sulfamidase expression in similar models. To achieve this, a batch of liposome nanoparticles was created encapsulating a designed, *SGSH*-carrying pDNA plasmid, analysed to ensure purity and appropriate properties, and used to transfect wildtype and MPS-IIIA human fibroblasts across multiple experiments. The transfected cells were tested for heparan sulfate levels, lysosomal storage, and autophagic activity. Additionally, a second, fresh batch of nanoparticles were prepared, analysed, and delivered into wildtype and MPS-IIIA disease model mice via intercranial injection. These mice were later euthanised and tissues

were collected. Brain samples were subsequently analysed for heparan sulfate levels and sulfamidase enzyme activity.

The results of the nanoparticle verification steps were positive, indicating an encapsulation ratio of approximately 80%, and a ~100-120nm size within the desired range indicted by the literature. However, the *in vitro* tests were only conducted for 4-day durations due to observed mortality in the initial experiment, and resulting *in vitro* data was inconclusive, with initial results not achieving statistical significance, and subsequent results indicating an increase in lysosomal storage and autophagic activity after treatment with the nanoparticle formulation.

This could be due to a mixture of variables potentially masking any treatment effects, such as lysosomal loading and induced autophagy due to cellular metabolism of lipid residues within the experimental timeframe, or oxidative stress affecting the outermost wells of treatment plates. Adjusted experimental designs with a focus on extended durations or randomisation could control for these factors, and modification of the liposome formulation could also be pursued to improve the encapsulation ratio further.

The *in vivo* experiments were conducted without issue, but failed to produce observable therapeutic effects or correction, indicating that further investigation into the stability, transfection efficiency, and expression of the encapsulated DNA nanoparticles may be required to determine the reason for the lack of effect.

Electronic Declaration

I certify that this thesis does not contain material which has been accepted for the award of any degree or diploma; and to the best of my knowledge and belief it does not contain any material previously published or written by another person except where due reference is made in the text of this thesis.

William Scott

Acknowledgements

Many thanks to my supervisors, Professor Kim Hemsley and Dr Adeline Lau, for the time and effort they have put into assisting me this past year. I started this project without any knowledge of the majority of techniques that I would end up carrying out, and their patient guidance and instruction was invaluable.

I would like to thank Dr Nicholas Smith from the Women's and Children's Hospital for his time, advice, and assistance with nanoparticle creation and quantitation methodologies.

I would like to thank the members of the Childhood Dementia Research Group (CDRG) lab for their advice, assistance, and clarifications regarding methods, equipment use, and reagent locations.

I would like to thank Dr Paul Trim and Dr Martin Snel from SAHMRI, for making time to help organise and assist my work there during the year.

I would like to thank Dr Nicholas Eyre and Pat Vilimas of the FMC microscopy unit for training and supporting me in the use of their equipment.

Finally, I would like to thank Professor Simon Conn and Dr Patricia Cmielewski for their time and effort as thesis assessors.

Introduction:

1.1 The Issue of Dementia

Dementia is an umbrella term used to refer to a common set of symptoms involving progressive impairment of reasoning, learning, and memory. The disorder can arise as a result of a variety of different neurological diseases, the most common being Alzheimer's disease, and individual risk increases with age (James & Bennet 2021).

Due to the severity of the symptoms, individual quality of life can be massively impacted. Dementia is a major cause of disability and dependency, and causes the seventh most deaths amongst all diseases (Global Burden of Disease collaborators 2021, World Health Organisation [WHO] 2021). In Australia, it causes the second most deaths out of all diseases (Australian Institute of Health and Welfare [AIHW] 2021).

Currently, over 55 million people suffer from dementia worldwide, and this number is expected to rise to 78 million by 2030 (WHO 2021). In Australia alone, over 400 thousand people suffer from dementia, and the friends and family of those with dementia are often impacted. It is estimated that 130 to 330 thousand Australians provide constant unpaid care to someone with dementia (AIHW 2021).

The annual economic burden of dementia is estimated at 1.3 trillion USD globally, and is projected to rise to over 2.8 trillion by 2030 (WHO 2021). Development of effective dementia treatments is complicated due to age-related complications in patients and the majority of dementia cases involving mixed pathologies, where symptoms arise due to multiple systematic issues in the patient (James & Bennet 2021).

While dementia mostly arises in older individuals, it can also arise during childhood as a result of rare genetic disorders (Hendricks *et al.* 2022, WHO 2021). These childhood dementia disorders are ideal candidates for research aimed at developing effective dementia treatments, due to their single-gene origin and the avoidance of age-related complications (James & Bennet 2021). One such single-gene disorder is MPS-III, otherwise known as Sanfilippo syndrome (Beneto et al. 2020).

1.2 Defining Sanfilippo Syndrome

Lysosomal storage disorders were first identified in the 1960s (Parenti *et al.* 2021). They consist of rare, inherited genetic disorders that result in impaired lysosomal metabolism and the accumulation of unprocessed metabolic by-products within tissues (Parenti *et al.* 2021, Beneto *et al.* 2020). The prevalence of lysosomal storage disorders in Australia is approximately 1 per 4800 births (Chin & Fuller 2022).

Mucopolysaccharidosis (MPS) are a subtype of lysosomal storage disorders specifically related to improper cellular processing of complex polysaccharide compounds known as glycosaminoglycans (Beneto *et al.* 2020). There are eight currently defined disorders within the group, and each relates to impaired processing of a specific glycosaminoglycan. In most of the disorders this is due to the absence or impairment of a single enzyme, however MPS III and IV are comprised of multiple subtypes (Muenzer 2011).

MPS disorders as a whole are usually characterized by progressive skeletal issues, joint problems, and degeneration of organ systems due to accumulation of unprocessed substrates within body tissues (Muenzer 2011).

MPS III, or Sanfilippo syndrome, was first characterized in 1963 and is comprised of four subtypes, each arising from a different single-gene mutation disrupting a step in the biological processing pathway for heparan sulfate, a glycosaminoglycan that has links to neurological growth (Beneto *et al.* 2020, Sanfilippo *et al.* 1963). Uniquely among the MPS disorders, the symptoms of Sanfilippo syndrome are primarily neurological in nature (Muenzer 2011).

As shown in Figure 1.1 below, Sanfilippo syndrome has an estimated prevalence of 1 case for every 70,000 births in Australia (Meikle *et al.* 1999), however it varies geographically, and some studies have estimated a lower global prevalence of approximately 1 case for every 130,000 births (Kong *et al.* 2021). The most common Sanfilippo subtype, MPS IIIA, has an estimated global prevalence of 1 per 200,000 births, and makes up over half the total number of Sanfilippo cases (Kong *et al.* 2021).

MPS IIIA arises due to mutation of the *N*-sulfoglucosamine sulfohydrolase (*SGSH*) gene, responsible for expression of the sulfamidase enzyme that catalyses the cleavage of sulfate groups from heparan sulfate during its degradation. Absence or loss of function of this enzyme thus results in disruption of that processing pathway, and the build-up of heparan sulfate in body tissues (Anthony 2015, Sidhu *et al*. 2014).

Figure has been removed due to copyright restrictions.

Figure 1.1: *Prevalence of Sanfilippo Syndrome (MPS III) and relative proportion of its subtypes, compared with the prevalence of MPS and lysosomal storage disorders overall (Sanfilippo Children's Foundation, 2019).*

1.3 Impacts of Sanfilippo Syndrome

Children born with Sanfilippo syndrome begin to show symptoms in early childhood, at approximately 2 to 4 years of age. These include learning difficulties, developmental delays, hyperactivity, and increased aggressiveness, and tend to present similarly across all subtypes of the disorder (Beneto *et al.* 2020, Valstar *et al.* 2011).

Due to the continual accumulation of heparan sulfate in tissues and the compounding damage this causes to the central nervous system, progressive loss of mental and motor functions is unavoidable without effective treatment (Beneto *et al.* 2020, Andrade *et al.* 2015, Valstar *et al.* 2011), as shown in Figure 1.2 below.

Life expectancy varies between subtype, with MPS IIIA being the most rapidly progressing form and having a life expectancy of approximately 15 years, while the rarer MPS IIIC has the highest life expectancy at approximately 23 years (Lavery *et al.* 2017). While the most impactful symptoms of Sanfilippo syndrome are primarily neurological in nature, other symptoms such as joint stiffness, difficulty swallowing, hearing loss, liver enlargement, and skeletal alterations can still occur, particularly in more pronounced cases (Beneto *et al.* 2020).

Removal of accumulated substrate via temporary interventions such as enzyme replacement therapy slows disease progression, but does not reverse existing damage (Beneto *et al.* 2020). Due to the early onset of the disease, along with early symptomatic similarity to more common neurological disabilities such as autism spectrum disorder, a child with Sanfilippo syndrome may suffer permanent neurological damage and impairment before receiving an accurate diagnosis, if proper newborn screening programs are not available (Schreck & Knapp 2022, Wolfenden *et al.* 2017).

Figure has been removed due to copyright restrictions.

Figure 1.2: *Outline of delayed developmental progression milestones and progressive impairment suffered by children with Sanfilippo syndrome, compared to a neurotypical child (Cure Sanfilippo Foundation, 2019).*

1.4 Current Treatment Landscape

Despite the severity of the disorder, there is currently no effective treatment for Sanfilippo syndrome (Beneto *et al.* 2020, Kong *et al.* 2020). However, there are a number of treatment avenues being actively researched, including enzyme replacement therapies, substrate reduction therapies, chaperone drug therapies, stem cell replacement therapies, and gene therapies (Kong *et al.* 2020, Penon-Portmann *et al.* 2023).

Enzyme Replacement Therapies

Enzyme replacement therapy (ERT) consists of directly replacing missing enzymes via injection into the bloodstream or cerebrospinal fluid. Due to the limited lifespan of the enzyme within the body, they require frequent, often weekly, repeated treatments to maintain enzyme levels. Additionally, the delivered enzyme has limited penetration into less vascular tissues such as bone, cartilage, or eyes. Despite these downsides, ERT therapies have been shown to have a treatment effect on highly vascular tissues and organ systems, and are available for several of the MPS disorders (Concolino *et al.* 2018, Penon-Portmann *et al.* 2023).

In the case of Sanfilippo syndrome, intravenous injection has limited efficacy due to the primarily neurological symptoms and the presence of the blood-brain barrier, while administration into the cerebrospinal fluid is much more invasive. As such, while some clinical trials are underway to investigate the use of ERT in MPS IIIA (Kong *et al.* 2020), alternative therapies that require less frequency or invasiveness may result in significantly greater quality of life for patients.

Substrate Reduction Therapies

Substrate reduction therapies usually involve the use of small molecule drugs that interfere with the production process of the targeted substrate, such as heparan sulfate, ideally reducing the rate of substrate production to a point where residual enzyme levels can properly degrade it. The most promising candidate drug for this was Genistein (Piotrowska *et al.* 2006), however subsequent clinical trials did not replicate the initial results, and did not show any treatment effect (Ruijter *et al.* 2011). As such, there is currently no drug shown to achieve this type of therapeutic effect in Sanfilippo syndrome (Penon-Portmann *et al.* 2023, Kong *et al.* 2020).

Chaperone Therapies

Chaperone therapies involve the regular use of small molecule drugs to stabilize existing enzyme or protect it from degradation, particularly in cases where the enzyme is present in the body but has misfolding errors that impact intra-cellular transportation and function. Due to being small molecules, chaperone drugs can also cross the blood-brain barrier, avoiding the need for invasive injection into the brain itself (Andrade *et al.* 2015). While this approach is limited in patients where the desired enzyme is entirely absent, chaperone therapies can also be used alongside enzyme replacement therapies, increasing the effective life of the delivered enzymes (Beneto *et al.* 2020, Diaz *et al.* 2020).

Stem Cell Replacement Therapies

Stem cell replacement therapies are expensive, invasive, and usually involve the transplantation of hematopoietic stem cells from a healthy donor, usually related, into the bone marrow of someone suffering from a disorder where it then should produce lineages of cells that are able to correctly express the missing enzyme. While this treatment has been effective in several types of MPS disorders, the primarily neurological nature of Sanfilippo syndrome means that the approach has seen minimal success, primarily limited to cases where transplantation was conducted at a very early age (Penon-Portmann *et al.* 2023, Khon *et al.* 2020).

Neuronal stem cells modified to express corrected levels of enzyme using lenti-viral vectors have been shown to be effective at correcting disease pathology in MPS-IIIB mouse models, and the technique is currently being trialled as a potential therapy in humans (Clarke *et al.* 2018). This approach could potentially be applicable to Sanfilippo syndrome as well. Research is also being conducted into deriving corrected neuronal cells from embryonic stem cells (Robinson *et al.* 2010).

Gene Therapies

Gene therapies involve using a vector to directly deliver genetic material into target cells for expression. In the case of Sanfilippo syndrome, the genetic material is usually designed plasmids containing a promoter compatible with human cellular machinery, an antibiotic resistance factor to allow verification of expression in cell models, and a wildtype version of the *SGSH* gene to allow the transfected cells to correctly express the impaired sulfamidase enzyme (Gill *et al.* 2009).

The choice of vector used in a gene therapy approach is highly important. Vectors should ideally be small in size to ensure optimal dispersion throughout tissues, stable for extended durations in appropriate cold storage conditions, and able to be degraded safely and completely by human cells after the genetic material is delivered (Laporte *et al.* 2006).

Viral vectors offer pre-existing candidates already adapted for such capabilities, and are the most commonly used vector for research and therapeutic applications. The primary viral vector studied for use in Sanfilippo syndrome is adenoviral-associated vector (AAV), a small, ~26 nm, vector widely used for gene therapy studies (Bulcha *et al.* 2021, Penon-Portmann *et al.* 2023, Wang *et al.* 2019). Prior studies have shown that these AAV vectors can be used to produce expression of sulfamidase in the brains of Sanfilippo mouse and large animal models, correcting many disease symptoms (Winner *et al.* 2016, Hocquemiller et al. 2020).

After being delivered into cells by an AAV vector, the SGSH gene is expressed in the cytoplasm. This means that cellular replication will not make additional copies of the introduced DNA, and repeated treatments would be required to maintain optimal gene expression as a patient grows. While some types of viral vector, such as lentiviruses, can integrate DNA directly into the nuclear genome of transduced cells, this carries the risk of inducing genetic errors, termed as insertional mutagenesis, that could lead to cancer (Bulcha *et al.* 2021).

Unfortunately, a major downside of viral vectors is their immunogenicity, meaning that repeated treatments will be progressively less effective, and the fact that a large portion of the population already carries antibodies against many common vectors (Shirley *et al.* 2020). One study relating to AAV vectors found that the occurrence of pre-existing neutralizing antibodies within a global child population could be as high as 70% for specific AAV serotypes, and no tested AAV serotype showed less than 38% of tested children with antibodies against it, as shown in Figure 1.3 (Rasko *et al*. 2022).

As such, alternative vectors or methods that could deliver designed plasmids into patient cells effectively, without such immunogenicity issues, would significantly advance our ability to provide proper treatment for Sanfilippo syndrome.

Figure has been removed due to copyright restrictions.

Figure 1.3: *Heatmap of neutralizing antibody prevalence against common AAV serotypes in global pediatric population, extracted 1:1 serum dilution section* (Rasko *et al.* 2022).

1.5 Potential of Nanoparticle Vectors

Lipid nanoparticles are an emerging area of research that offer an alternative gene therapy vector. They are comprised of DNA plasmids encapsulated by polar lipids in small nanoparticles, and are self-forming due to relative charges under the right conditions. These particles allow delivery and cellular uptake similar to a virion capsid, and both size and chemical properties can be adjusted based on the lipid composition used in the nanoparticle's creation (Tomsen-Melero *et al.* 2022, Albertson *et al.* 2022).

Existing liposome and lipid nanoparticle formulations for drug delivery and gene therapy primarily utilize a few common types of lipids, specifically an ionizable cationic lipid such as DODAC, a polyethylene glycol-lipid conjugate such as DMPE-PEG to reduce aggregation, and various other lipids useful for structural stability, such as cholesterol or DOPE (Albertson *et al.* 2022, Kauffman *et al.* 2015).

These nanoparticles are effective at protecting nucleic acids from degrading and are non-immunogenic, a critical aspect for the potential to be an alternative to established viral vector techniques (Tomsen-Melero et al. 2022). If shown to be an effective gene therapy vector that can induce therapeutic levels of sulfamidase expression in Sanfilippo syndrome, these properties would allow repeated treatments over a patient's lifespan without loss of efficacy, as well as being usable in the large portion of patients who carry pre-existing antibodies against AAV vectors even before initial treatment. This may lead to the first reliable treatment for the disorder.

Additionally, a working vector design could be utilized with pDNA payloads tailored for the treatment of other lysosomal storage disorders or diseases arising from single-gene mutations, particularly in cases where repeat treatments are required, or the immunogenicity of viral vectors is an issue.

1.6 Existing Work

Prior studies within the Childhood Dementia Research Group have resulted in the design of a *E.coli* raised, *SGSH*-carrying pDNA plasmid using a CMV-IE promoter sequence for widespread expression throughout body tissues. This plasmid was used to transfect HEK-293 cells *in vitro* using lipofectamine, and as shown in Figure 1.4, treated cells showed a 49-fold increase in sulfamidase activity compared to controls, verifying the efficacy of the plasmid (*Childhood Dementia Research Group, unpublished data*).

Additionally, work between the CDRG lab and collaborators formulated the composition and preparation methods for producing pDNA-encapsulating lipid nanoparticles. These liposomes were used to deliver plasmids encoding green fluorescent protein (GFP) into the brains of six wildtype mice at 6 weeks of age. The mice were then euthanized 4 weeks post-treatment and later histological analysis of brain samples from those mice showed widespread expression of the green fluorescent protein throughout the brain tissues (see Appendix A), indicating that the liposome formulation was effective as a gene therapy vector (*Childhood Dementia Research Group, unpublished data).*

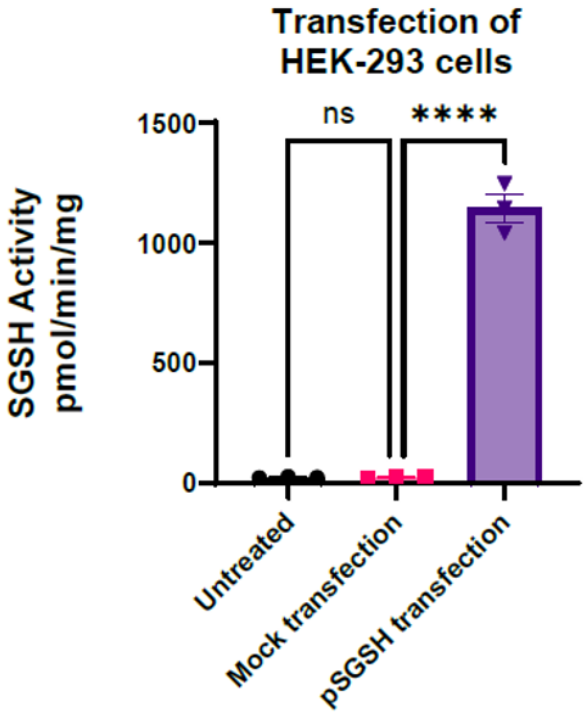

Figure 1.4: *SGSH enzyme activity of HEK-293 cells 48 hours after transfection with 800ng SGSH-gene-carrying pDNA plasmid, an equivalent volume of media and transfection reagents, or no treatment. Enzyme quantified via co-incubation of sonicated cells samples with fluorogenic SGSH substrate and measurement of 360 nm emission, 460 nm excitation on a SpectraMax iD5 plate reader (Childhood Dementia Research Group, unpublished data).*

1.7 Project Overview

This project aims to use the confidential liposome formulation to encapsulate the designed *SGSH*-encoding pDNA plasmid, verify the quality and safety of the nanoparticles, and explore its therapeutic effectiveness *in vitro* and *in vivo*.

The cell lines used by the project are human fibroblasts, specifically GM38 wildtype and GM6110 MPS-IIIA disease model cell lines, with the GM6110 cell line featuring a G>A mutation at nucleotide 746 in the SGSH gene. Fibroblasts were chosen due to ease of culturing compared to neuronal cells, combined with a high familiarity with managing them in the CDRG Lab.

The mouse strains used by the project are wildtype C57BL/6 mice and congenic MPS-IIIA disease model variants of that wildtype strain, featuring a D>N mutation at nucleotide 31 and a G>A mutation at nucleotide 91 in the SGSH gene. All mice are from lineages isolated in Adelaide and maintained by the CDRG Lab (Crawley *et al.* 2006). The targeted regions for nanoparticle delivery are the thalamus and striatum of the brain, chosen due to central placement, prior precedent with AAV studies (Hocquemiller *et al.* 2020), and density of natural transport networks.

Quantitation will be carried out via established methods for measuring heparan sulfate levels in cell or tissue homogenate using liquid chromatography and mass spectroscopy (He *et al.* 2019), or via sulfamidase enzyme activity assay (Whyte *et al.* 2015, Karpova *et al.* 1995).

1.8 Research Hypothesis and Aims

The hypothesis is that the lipid nanoparticles will allow effective delivery of the pDNA plasmid and expression of the target sulfamidase enzyme in both Sanfilippo cell and mouse models, correcting the disease phenotype and indicating a potential therapeutic avenue for the disease.

To achieve this, the following aims will be pursued:

Aim 1: To create pDNA-containing lipid nanoparticles and verify encapsulation, size, and concentration are suitable for use in experiments.

Aim 2: To treat human fibroblast cell lines with the nanoparticles and test for therapeutic effect *in vitro*.

Aim 3: To treat disease-model mice with the nanoparticles to verify therapeutic effectiveness *in vivo*.

Materials & Methods:

2.1 Reagents & Materials

Table 1: Reagent consumables used in project.

Reagent	Supplier	Additional Information
2,2-dimethoxypropane	Sigma Aldrich	Cat: D1386808-25ML
40X custom Taqman SNP genotyping assay	Life Technologies	Cat: 4332075
4-Methylumbelliferyl N-sulpho-α-D-glucosaminide (MU-αGLcNS) 2.2 mg/ml	Carbosynth	Cat: EMO6602
4-MU standard	Sigma Aldrich	Cat: M1381
Anti-p62 SQSTM1 Monoclonal Antibody	Abnova	Cat: H00008878-M01
BCA Micro – Protein Assay Kit	Thermo Fisher Scientific	Cat: 23235
Butanolic Hydrochloric Acid	Sigma Aldrich	Cat: 87472-50ML-F
Chelex-100 (10%)	BioRad	Cat: 142-1253
Deuterated HS internal standard (n-butyl (2-amino-2-deoxy-α-D-glucopyranosyl)-(1→4)-(n-butyl-d9 α-D-glucopyranosid)uronate) (100 ng/ml)	University of Queensland	Prepared in collaborator lab; Prof Vito Ferro, University of Queensland.
Dimethylsulfoxide (DMSO)	Sigma Aldrich	Cat: 34869-1L
Di-sodium hydrogen orthophosphate	Chem Supply	Cat: SA026
DNA Standard Ladder pUC19	Geneworks	Cat: DMW-P1, 500ng/µl
Ethanol (100%)	Chem Supply	Cat: EL027-10L-P
Ethylenediaminetra-acetic acid (EDTA)	AnalaR	Cat: 100093.3T
Fetal Calf Serum (FCS)	Bovogen	Cat: SFBS-F
Formalin / Formaldehyde (37%)	Chem Supply	Cat: FA010-500M
Glacial acetic acid	Univar	Cat: UN2789
Heparan sulfate salt for HS assay (1 µg/ml)	Celsius Laboratories	Cat: HO-3105
HEPES	Formedium	Cat: HEPES05
Hoechst stain	Sigma Aldrich	Cat: 14523-100MG
Human fibroblast cell line (MPS IIIA model)	Coriell Institute	Cat: GM06110
Human fibroblast cell line (wildtype model)	Coriell Institute	Cat: GM00038
Hydrochloric Acid	Scharlau	Cat: AC07412501
Isopropanol alcohol	Chem Supply	Cat: PA013-2.5L-P
L-Glutamine 5000	Sigma Aldritch	Cat: G7513-500ML
Lipid Stocks	Confidential	Confidential
Lysotracker Red – 1 mM stock	Thermo Fisher Scientific	Cat: L7528
McIlvaine's phosphate/citrate buffer (Pi/Ci buffer)	CDRG Lab	Prepared in lab via method 2.2.10
Milli-Q purified water	Flinders University	Purified on-site
Minimum Essential Medium Eagle (EMEM)	Sigma Aldrich	Cat: M5650
Mouse secondary antibody, FITC-conjugated	Jackson Immuno Research	Cat: 715-545-150
Normal Donkey Serum (NDS)	Jackson Immuno Research	Cat: 017-000-121
Paraformaldehyde (PFA) powder (pre-mixed)	Sigma Aldrich	Cat: P6148-1kg
Penicillin-Streptomycin solution (Pen-Strep)	Thermo Fisher Scientific	Cat: 15140122
Phosphate Buffered Saline (Dulbecco's PBS)	Thermo Fisher Scientific	Cat: 14190250

Plasmid DNA stocks	CDRG Lab	Prepared by the Gene Silencing and Expression Core Facility, The University of Adelaide
Potassium chloride	AnalaR	Cat: 10198
Potassium dihydrogen orthophosphate	Chem Supply	Cat: PA009
Quality control sample for BCA assay	CDRG Lab	Prepared in lab from mouse brain homogenate.
Quality control sample for HS assay	CDRG Lab	Prepared in lab from MPS-IIIA mouse brain homogenate.
Quant-iT PicoGreen dsDNA Reagent	Thermo Fisher Scientific	Cat: P7581
Recombinant Human Sulfamidase/SGSH Protein	R&D Systems	Cat: RDS4119GH010
Sodium Acetate	Chem Supply	Cat: SA005-500G
Sodium Chloride	Chem Supply	Cat: SA046-3KG
Sodium Hydroxide	Chem Supply	Cat: SA178-500G
Taqman Genotyping Mastermix	Life Technologies	Cat: 4371353
Tris(hydroxymethyl)-aminomethane (Tris)	Formedium	Cat: TRIS01
Trisodium Citrate Dihydrate	MERCK	Cat: A763248
Triton-X100	Sigma Aldrich	Cat: 9002-93-1
Trypan Blue dye solution (0.4%)	Sigma Aldrich	Cat: T8154-100ML
Trypsin-EDTA (0.5%) solution 10x	Sigma Aldrich	Cat: 59418C-100ML
α-Glucosidase	Sigma Aldrich	Cat: G3651

Table 2: Material consumables used in project.

Material	Supplier	Additional Information
15 ml Amicon® Ultra centrifugal filters	Merck Millipore	Cat: UFC901008
2 ml tubes – Fast Prep-24, Lysing matrix D	MP Biomedicals	Cat: 116913-500
96 well microplate, black wells with clear bottoms.	Greiner Bio-one	Cat: 655096
96 well microplate, clear, flat bottom.	Greiner Bio-one	Cat: 655101
Cryotubes – sterile polypropylene screw cap	Proscitech	Cat: YT340-12R
Dental Needles - 27G Morita	SSS Australia	Cat: 1456504
Hypodermic needles – 25G	Beckton Dickinson	Cat: 301807
Isopropanol Freezing Container - 'Mr Frosty'	Nalgene	Cat: 5100-0001
MicroAmp 0.1 ml 96 well plate - genotyping	Life Technologies	Cat: 4346907
Plate sealer, adhesive back	MP Biomedicals	Cat: 76-401-05
SpectraPor 1 dialysis membrane – 6-8 kD MWCO	Spectrum	Cat: 132655
Syringe – single use 1 ml	Beckton Dickinson	Cat: 302100
Syringe filters (Minisart® 0.2 µm)	Sartorius	Cat: 16534-K
Tissue culture flask – 25cm^2	Corning	Cat: 430639
Tissue culture flask – 75cm^2	Corning	Cat: 430641U
Tissue culture plate – 24 well	Costar	Cat: 3524
Tissue culture plate – 48 well	Costar	Cat: 3548
Tissue culture plate – 96 well	Costar	Cat: 3599

For preparation of chemical reagents, buffers, and fixatives, see Appendix B.

2.2 Methods for Nanoparticle Creation and Quality Control.

2.2.1 Preparation of designed pDNA plasmid

The pDNA plasmid was designed in-lab to express the human N-sulfoglucosamine sulfohydrolase (*SGSH*) gene in order to produce the sulfamidase enzyme. It was derived from *E.coli* and uses a CMV-IE promoter sequence.

Attribution: Design and construction of the *SGSH*-encoding pDNA plasmid was carried out by Dr Adeline Lau.

2.2.2 Preparation of pDNA in Citrate Buffer

Designed 4.6 mg/ml pDNA plasmid solution was combined with prepared 4ºC 10 mM Citrate Buffer at a ratio of 0.87 µl per ml, to produce a 4 ng/ml solution.

2.2.3 Preparation of Cationic Liposomes with Encapsulated pDNA

Prepared pDNA and Citrate buffer was aliquoted into 2ml microfuge tubes, vortexed, and centrifuged at 13,000g for 10 minutes using a Heraeus Biofuge-pico centrifuge. Supernatant was recombined and passed through a 0.2 µm Sartorius Minisart® filter three times, before being split into 1.1 ml aliquots and heated on a heating block to 37ºC for 10+ minutes. A preparation of commercial lipid stocks was also prepared, split into aliquots, and heated (*details withheld*).

pDNA + Citrate aliquots were held on a vortex to induce laminar flow for an extended duration, and a volume of the lipid preparation was injected directly into the centre of the vortex over two seconds. The vortex was then sustained for 10 seconds to ensure effective nanoparticle formation before the combined aliquot was removed. All combined aliquots were merged and passed three times through clean 0.2 µm Sartorius Minisart® filters, with sterile citrate buffer used as a wash for the final filter pass. Nanoparticle solution was then stored at 4ºC.

Attribution: Preparation of lipid nanoparticles was carried out with assistance from Dr Nicholas Smith and Dr Adeline Lau. Size-testing of lipid nanoparticles was carried out by Dr Nicholas Smith using a Malvern Zetasizer.

2.2.4 Filtering and Concentration of Cationic Liposomes with Encapsulated pDNA

Nanoparticle preparation was transferred equally into two Amicon Ultra 15 ml centrifugal filters, and spun at 3,270g using a Beckman Coulter Algeria™ X-12R centrifuge until 1 ml of retentate remained. The centrifugation process was repeated after the addition of 11 ml sterile

10 mM Citrate Buffer, then 11 ml sterile HEPES buffered saline, and finally 11 ml sterile PBS. After all steps, eluate was transferred into clean 50 ml falcon tubes and stored at 4°C. The final nanoparticle retentate was transferred into a sterile microfuge tube and stored at 4°C.

2.2.5 Quantitation of Nanoparticle pDNA encapsulation ratio via PicoGreen assay

PicoGreen assay was prepared on black, clear-bottom 96 well microplate with pUC19 DNA standard ladder as reference. Nanoparticle retentate samples plated in duplicate at 1:10 and 1:20 concentrations diluted in TE buffer, and with 100 ul of 1:200 diluted PicoGreen reagent added to all wells. Fluorescence was read after 5-min dark incubation on a Spectramax iD5 plate reader at 485/535 nm.

After initial reading, all wells received 2 µl 10% (v/v) Triton-X100 to disrupt liposome encapsulation and were incubated in the dark for 10 mins, before being read again.

Total DNA was determined by creating a standard curve using the DNA standard dilutions, using the standard curve equation to find the per-well concentration of each sample in ng/ml, converting that to ng/µl, accounting for the dilution factors.

The percentage change in encapsulation was then determined by dividing the initial total DNA by the total DNA after the liposomes were disrupted with Triton-X100, and multiplying by 100 to obtain a percentage. The initial percentage encapsulation can then be determined by subtracting that result from 100.

2.3 Methods for Cell Experiments.

2.3.1 General methods

2.3.1.1 Maintenance of fibroblast cell lines

GM38 (wildtype) and GM6110 (MPS-IIIA disease model) fibroblast cell lines were cultured in 25cm^2 and 75cm^2 Corning tissue culture flasks, with 5 or 12 ml of growth media (depending on flask size), in a Napco 5100 cell culture incubator maintained at 5% CO_2, 37°C. Cell culture confluence and health was examined using a Leitz Diavert inverted light microscope daily, and growth media was changed weekly.

2.3.1.2 Splitting and passaging fibroblast cell lines

Cell growth media was aspirated via a glass Pasteur pipette and the cell layer washed twice with sterile PBS. Cells were induced into suspension via addition of 10% Trypsin-EDTA, a 5-minute incubation, and mechanical agitation. Growth media was added at to inactivate

Trypsin at a ratio of 1 ml media for every 2 ml of Trypsin, and the cell suspension was transferred into a 10 ml tube and centrifuged at 350g for 5 minutes using a Beckman Coulter Algeria™ X-12R centrifuge. Supernatant was aspirated and cells resuspended gently in 1 ml of media for counting and subsequent seeding or freezing.

2.3.1.3 Cell counting via Trypan Blue method

10µl of the resuspended cell solution is combined with 10 µl 0.4% Trypan Blue dye and thoroughly mixed via pipette. 10 µl of this solution was then pipetted into both chambers of a Hausser Scientific improved neubauer haemocytometer, and the cells in the central intersecting grid square counted and averaged between chambers. The number of counted cells was then multiplied by $2x10^4$ to obtain the number of cells/ml.

2.3.1.4 Freezing and Thawing fibroblast cell lines

Resuspended cell solutions were pooled after an aliquot was counted, and the combined pool was centrifuged at 350g using a Beckman Coulter Algeria™ X-12R centrifuge for 5 minutes. Supernatant was removed and cell pellet resuspended in cell growth media containing 5% DMSO, targeting a concentration of over $1x10^6$ cells/ml. Readied cryovials then received 1ml aliquots of this solution and were inserted into a 'Mr Frosty' slow-freezing isopropanol bath and placed into a -80^{o}C fridge overnight, before being transferred to LN2 storage.

To thaw cell stocks, cryovials were placed into a 37^{o}C water bath and agitated vigorously as soon as possible after removal from LN2 storage. Once completely thawed, the cryovial exteriors were swabbed with 70% ethanol and the vials moved into a sterile tissue culture hood to be transferred gently into a 10 ml tube. An additional 9 ml non-DMSO cell growth media was added dropwise, and the tube was centrifuged at 350g for 5 minutes at room temperature, using the same Beckman Coulter Algeria™ X-12R centrifuge. Supernatant was discarded and cells were resuspended in 1 ml growth media for standard counting and seeding methods.

Cell growth media was changed for fresh media 24 hours after being thawed and seeded.

2.3.2 Experiment 1: The effect of nanoparticle treatment on cellular heparan sulfate.

2.3.2.1 Seeding and treatment of experimental culture plate

A sterile, clear 24 well culture plate was seeded with 3 wells of GM38 human fibroblasts and 21 wells of GM6110 human fibroblasts, at a density of $5x10^4$ cells per well in 500 µl growth media. The plate was then incubated in a Napco 5100 incubator at 5% CO_2, 37ºC overnight to allow the cells to adhere. The cells were then treated the next day.

The treatment groups consisted of three GM6110 groups treated with unencapsulated pDNA at 0.5, 1, and 2 pg/cell concentrations, and three GM6110 groups treated with liposome nanoparticles at 0.5, 1, and 2 pg/cell concentrations. GM38 and GM6110 wells treated with media containing only sterile PBS were used as controls. All treatment groups consisted of three replicate wells on the same plate.

The seeding growth media was aspirated from the plate wells and replaced with 500 µl of an appropriate treated media solution. The culture plate was then placed back in a 5% CO_2, 37ºC Napco 5100 incubator to grow for 4 days, due to observed toxicity effects in 2pg/cell DNA and Nanoparticle corner wells precluding a 7-day growth duration.

Table 3: Cell line & treatment type layout for heparan sulfate cell experiment.

	GM38 PBS			GM6110 PBS	
	GM6110 0.5pg/cell DNA			GM6110 0.5pg/cell Nano	
	GM6110 1pg/cell DNA			GM6110 1pg/cell Nano	
	GM6110 2pg/cell DNA			GM6110 2pg/cell Nano	

2.3.2.2 Cell harvest from treatment plate

The growth media in each well was removed and each well was washed gently with 500 µl sterile PBS twice, before 250 µl 10% Trypsin-EDTA was added, and the plate was incubated for 5 minutes. After incubation, 250 µl growth media was added to each well to inactivate the trypsin and the contents of each well was transferred to a 10 ml tube and centrifuged at 350g for 5 minutes using a Beckman Coulter Algeria™ X-12R centrifuge. Supernatant was removed and 1 ml sterile PBS added to each tube before the centrifugation was repeated. PBS supernatant was then removed and 100 µl Tris-NaCl added. Samples were then sonicated for 20 seconds and immediately stored on ice.

2.3.2.4 Sample preparation for heparan sulfate assay

A Thermo Fisher Scientific Micro-BCA protein assay kit was used to determine the protein concentration of the sonicated cell samples, using dilutions of its provided bovine serum albumin as standards on a clear, flat bottom 96 well microplate. The cell samples were plated in duplicate, with 15 µl sample to 85 µl Milli-Q water. 100 µl of the mixed BCA reagent was added to each well, and the plate was incubated for 2 hours at 37ºC before excitation was read at 562 nm.

The BCA data was used to determine the protein concentration of each sonicated cell sample, so that a volume of the sample totalling 5 µg protein could be aliquoted into a clean glass test tube, with Tris-NaCl buffer used to ensure a uniform total volume. These samples were then freeze-dried using a Christ-Vaccubrand vacuum concentrator and stored at -20ºC.

2.3.2.5 Butanolysis assay of cell heparan sulfate storage

Based on an established methodology (He *et al.* 2019) 50 µl 2,2-dimethoxypropane was added to each of the dried-down samples in a fumehood, followed by 1 ml 3M butanolic HCl using a positive displacement pipette. Test tube lids were then secured tightly, and the tubes incubated at 100ºC for 2 hours in a heating block.

After 2 hours, the temperature of the heating block was lowered to 45ºC, and the test tube lids removed and placed down in clear order. An improvised nitrogen dry-down system was then used to completely dry all tubes over several hours. Each tube then received 200 µl HS internal standard solution and was briefly vortexed, then centrifuged at 13,000rpm in a Heraeus benchtop centrifuge in two brief pulses.

Samples were placed in a rotary shaker for 30 minutes at room temperature, before being pulse-centrifuged again and transferred into a 600 µl Eppendorf tube. The tubes were then centrifuged at 13,000rpm for 15 minutes using a Heraeus Biofuge-pico centrifuge, and 150 µl supernatant transferred into a well in a clear 96 well plate. Standards, Milli-Q water blanks, and internal quality control replicates were then plated at the same volume, and the plate was sealed using a foil heat seal.

2 µl injection volumes of each sample underwent liquid chromatography separation using an Acquity UPLC equipped with a 2.1 mm ID x 50 mm BEH C18 (1.7 µm particle-size) analytical column at a flow rate of 350 µl per minute, using two solvents comprised of water or acetonitrile each containing 0.1% formic acid.

Mass spectrometry analysis of separated samples was carried out using a API 4000 QTrap spectrophotometer in multiple reaction monitoring mode. Samples were analysed in a random order, and a blank injection of sterile water was used every 4th injection. Transitions were monitored at 50 millisecond scan-times, and the peak areas were calculated using Analyst 1.6.2. The peak relating to the GlcN α1-6 GlcUA disaccharide was used as marker for total heparan sulfate content.

Attribution: Liquid chromatography and mass spectrometry methods were carried out by Dr. Paul Trim and Dr. Marten Snel at SAHMRI, as per established methods (He *et al.* 2019).

2.3.3 Experiment 2: The effect of nanoparticle treatment on cellular lysosomal size.

2.3.3.1 Seeding and treatment of experimental culture plate

A sterile, clear 96 well culture plate was seeded with 6 wells of GM38 human fibroblasts and 13 wells of GM6110 human fibroblasts, at a density of $1.5x10^4$ cells per well in 100 µl growth media. The plate was then incubated overnight in a Napco 5100 incubator maintained at 5% CO_2, 37^{o}C, to allow the cells to adhere and be treated the next day.

The treatment groups consisted of two GM6110 groups, comprised of 4 wells each, treated with liposome nanoparticles at 2 and 4 pg/cell concentrations. GM38 and GM6110 wells treated with media containing only sterile PBS were used as controls. Additional replicates were included to serve as unstained or media-only controls.

The seeding growth media was aspirated from the plate wells and replaced with 100 µl of an appropriate treated media solution. The culture plate was then placed back in the 5% CO_2, 37^{o}C incubator to grow for 4 days, to match the duration of the earlier heparan sulfate experiment.

Table 4: Cell line & treatment type layout for lysosomal storage size experiment.

GM38 PBS			
GM6110 PBS			
GM6110 2pg/cell Nano			
GM6110 4pg/cell Nano			

2.3.3.2 Fixation and lysotracker staining of treatment plate

Growth media in each well was aspirated and replaced with 100 µl 75 nM Lysotracker Red diluted in 37ºC cell growth media. The plate was then incubated in a Napco 5100 incubator maintained at 5% CO_2, 37ºC for 1 hour, had the treated media aspirated, and was gently washed with 100 µl sterile PBS twice.

After aspiration of the second PBS wash, each well received 100 µl chilled 4% PFA solution and was incubated for 10 minutes at room temperature. Following the incubation, the PFA solution was aspirated, and the plate was washed with sterile PBS two more times.

After aspiration of the last PBS wash, each well received 100 µl 0.05% Hoechst nuclear stain in sterile PBS and was again incubated for 10 minutes at room temp, before receiving two more PBS washes and being stored at 4ºC.

2.3.3.3 Imaging and analysis of Lysotracker-stained cell plate

The stained plate was visually imaged using an Olympus IX83 inverted microscope at 20x magnification and its 500nm and 365nm LEDs set at 30% intensity. The lysotracker stain was imaged at a 550 nm wavelength and a 600 ms exposure time, with an EM gain of 30. The brighter Hoechst stain was imaged at a 365 nm wavelength with an exposure time of 200 ms and an EM gain of 14.

Quantitative analysis of the stained plate was carried out using a Spectramax iD5 plate reader to read fluorescence at 577-617 nm for the Lysotracker stain and 346-460 nm for the Hoechst stain. For each well, dividing the value obtained for the lysotracker stain by the value for the Hoechst stain gives a numerical indication of the lysosomal storage volume per cell.

2.3.4 Experiment 3: The effect of nanoparticle treatment on cellular autophagy.

2.3.4.1 Development of immunostaining method

A method was investigated to achieve clear and distinct staining of human fibroblast cells using primary antibodies specific to autophagic markers, and fluorophore-conjugated secondary antibodies.

Clear, 96 well test plates were seeded with GM38 and GM6110 human fibroblasts and allowed to adhere, before being fixed, stained with a selection of candidate primary antibodies, incubated overnight, stained with corresponding secondary antibodies, nuclear stained, and imaged using various settings.

The Olympus IX83 inverted microscope was initially used, however a simpler EVOS fluorescence microscope was found to produce quality images with easier and faster operation.

There were three main antibody stains tested, specifically an anti-LC3B polyclonal primary antibody combined with a Cy3-conjugated rabbit secondary antibody, an anti-p62 monoclonal primary antibody combined with a FITC-conjugated mouse secondary antibody, and an anti-p62 ICK monoclonal primary antibody combined with the same FITC-conjugated mouse secondary antibody.

Multiple control factors were included in the tests, including unstained wells, wells without cells that went through all fixing and staining steps, primary-only wells, secondary-only wells, and wells treated with non-compatible or both types of secondary antibodies.

Each antibody was additionally tested at multiple concentrations, at 1:1000, 1:500, 1:200, 1:100, and 1:50 dilution concentrations.

All wells were imaged in Hoechst-corresponding DAPI, Cy3-corresponding RFP, and FITC-corresponding GFP color channels at multiple light intensities using the EVOS microscope.

The anti-p62 primary antibody performed the best out of all the tests, and optimal signal was obtained at 1:50 concentration, 80% GFP channel intensity. The anti-LC3B antibody performed less effectively, with visible but limited staining in the RFP color channel at higher concentrations and intensities, while the anti-p62 ICK primary antibody failed to produce clear staining across any test.

2.3.4.2 Seeding and treating of experimental culture plate

A sterile, clear 96 well culture plate was seeded with 5 wells of GM38 human fibroblasts and 20 wells of GM6110 human fibroblasts, at a density of $1.5x10^4$ cells per well in 100 µl growth media. The plate was then incubated overnight at 5% CO_2, 37ºC to allow the cells to adhere and be treated the next day.

The treatment groups consisted of four GM6110 groups, comprised of 6 wells each, treated with liposome nanoparticles or unencapsulated pDNA at 2 and 4 pg/cell concentrations. GM38 and GM6110 wells treated with media containing only sterile PBS were used as controls. Additional replicates were included to serve as unstained, primary-antibody-only or secondary-antibody-only controls.

The seeding growth media was aspirated from the plate wells and replaced with 100 µl of an appropriate treated media solution. The culture plate was then placed back in a 5% CO_2, 37ºC incubator to grow for 4 days, to match the duration of the earlier heparan sulfate experiment.

Table 5: Cell line & treatment type layout for p62 immunostaining cell experiment

		GM38 PBS		
		GM6110 PBS		
		GM6110 2pg/cell DNA		
		GM6110 4pg/cell DNA		
		GM6110 2pg/cell Nano		
		GM6110 4pg/cell Nano		

2.3.4.3 Fixation of treatment plate

The experimental plate was removed from the incubator and moved into a fumehood where the growth media was carefully aspirated, and the wells were gently washed once with 100 µl sterile PBS. The PBS was then aspirated, and each well received 100 µl cold 4% paraformaldehyde in PBS.

After 10 minutes had passed, the paraformaldehyde was removed and disposed of appropriately, and each well received 100 µl sterile PBS that was gently used to wash the cells. The plate then sat for 5 minutes at room temperature before the PBS was removed and a fresh 100 µl PBS was added to repeat the process.

After the third PBS wash, the plate was ready to either receive another 100 µl PBS in each well and be stored at 4^{o}C, or to immediately undergo primary staining.

2.3.4.4 Primary staining of treatment plate

Each well had any remaining PBS carefully aspirated, and 100 µl 0.3% Triton-X100 in PBS was added. After sitting for 5 minutes at room temperature, the Triton-X solution was removed, and each well was washed three times with cold, sterile PBS as per the prior steps, with each wash being allowed to sit for 5 minutes at room temperature before being replaced.

After the wash process, each well received 100 µl of a blocking solution comprised of 10% normal donkey serum and 0.03% Triton-X100 in PBS. The plate was then allowed to incubate at room temperature for 1 hour.

After incubation, the blocking solution was removed and replaced with 100 µl of a primary antibody solution containing 2 µl Anti-p62 SQSTM1 monoclonal antibody and 4 µl normal donkey serum in PBS. The experimental plate was then incubated a Napco 5100 incubator maintained at 5% CO_2, 37^{o}C overnight.

2.3.4.5 Secondary staining of treatment plate

After overnight incubation, the primary antibody solution was removed and each well was washed three times with 100 µl cold sterile PBS as per prior steps, again allowing 5 minutes at room temperature between each wash.

After the washing steps were completed and any remaining PBS was removed, 100 µl 1:200 diluted FITC-conjugated mouse secondary antibody in PBS was added to each well. The experimental plate was then incubated in the dark for 3 hours at room temperature, wrapped in aluminium foil.

After incubation with the secondary antibody each well was washed three times with PBS, with the plate wrapped in foil for each 5-minute rest step. After the last PBS was removed, each well received a 1:2000 dilution of Hoechst nuclear stain in PBS and was incubated in the dark at room temperature for 10 minutes. After incubation, another three PBS wash steps were carried out, and a final 100 µl PBS added to each well for the imaging process.

2.3.4.6 Imaging of stained plate

Stained experimental plate was imaged using an EVOS fluorescence microscope at 40x magnification, using the GFP green colour channel at 80% intensity to image the antibody staining, and the DAPI blue colour channel at 50% intensity to image the nuclear staining.

Five locations were imaged from each well, and each location was imaged using the GFP and DAPI channels separately, resulting in 10 images per well and 50 images per treatment type.

2.3.4.7 Quantitative analysis of immunostaining images

Images were processed using ImageJ 'FIJI' software package. Hoechst-stained nuclei were manually counted via placing automatically incrementing markers using the software's star tool, where the density was distinguishable. In cases where the cells were too dense for accurate manual counting, that over-dense area was drawn around, highlighted, and excised from that well location, for both the DAPI and GFP channel images.

After manual counting of the nuclei present in the DAPI channel image of the location, the GFP channel image was processed automatically via the following steps: Background signal was removed via 'Process > Subtract background: 10 pixels', Image was converted using 'Image > Type > 8 bit', Image was adjusted using 'Image > Adjust > Threshold: 10-225', and the signal was quantified using 'Analyze > Measure' to determine the percentage area of showing antibody signal above the defined threshold.

That percentage area was then divided by the number of nuclei counted for that well location, to obtain a quantified value for antibody signal per cell.

2.4 Methods for Mouse Experiments

2.4.1 Experiment 4: Treatment, Observation, and Harvest of Mouse Cohort

2.4.1.1 Treatment of Mice via Intercranial Injection

A cohort of 5 wildtype and 15 MPS IIIA disease model mice received a once-off set of intraparenchymal injections at an age of 6 weeks. The injections were made via stereotaxic infusion at flow rate of 0.5µl per minute, using 27G Morita dental needles, into 4 total injection sites, two on each side of the brain. The primary target regions were the thalamus and striatum, and a 0.75µl volume was delivered into each site at two depths, making for a total injection volume of 1.5µl per site, and 6µl per mouse.

The solution delivered was dependent on the specific treatment groups:

- 5x wildtype mice received PBS vehicle solution as controls.
- 5x MPS IIIA disease model mice received PBS vehicle solution as controls.
- 5x MPS IIIA disease model mice received unencapsulated pDNA plasmids in PBS solution, with a targeted dose of $5x10^{12}$ plasmid copies per kg of bodyweight.
- 5x MPS IIIA disease model mice received liposome nanoparticles containing pDNA plasmids, in PBS solution, with an equivalent dose target to the unencapsulated plasmids.

Attribution: Surgical treatment of mice was carried out by Professor Kim Hemsley.

2.4.1.2 Observation of Treated Mice

Treated mice were initially checked at 2, 24, 48, and 72 hours post-surgery following a clinical record sheet (CRS). This monitoring involved observation of mouse activity, weight, posture, coat condition, breathing, and any signs of discharge, injury, or discomfort.

After this period, the treated mice were observed daily for behavioural or physical abnormalities, and the detailed CRS checks were carried out on a weekly basis, until the end of the 4-week experimental duration.

If a mouse showed any signs of distress, injury, or weight loss, it was checked twice daily until its condition improved.

Attribution: Post-treatment monitoring of mice was carried out primarily by Professor Kim Hemsley and Dr Adeline Lau.

Figure has been removed due to copyright restrictions.

Figure 2.4.1: *Diagram of mouse brain regions with injection sites indicated. Brain diagram sourced from GENSAT project, Rockfeller University.*

2.4.1.3 Euthanasia and Sample Collection

After reaching 10 weeks of age (4 weeks post-treatment) mice underwent a routine CRS check before euthanasia and were humanely euthanized via CO2 asphyxiation in a clear, sealed box. A tail-pinch test was used to confirm a lack of response before proceeding, and time of death was recorded. Ear samples were taken with sterile surgical scissors and stored at for -20^{o}C later genotyping.

A cardiac bleed was conducted using a sterile, 25G single-use hypodermic needle and 1 ml syringe. The needle was removed to deliver the blood into a pre-labelled, sterile, screw-capped 1.5 ml microfuge tube without lysis, and the blood was then allowed to sit for 30 minutes at room temperature before being centrifuged at 13,000g in a Heraeus Biofuge-pico centrifuge for 15 minutes. Supernatant was then transferred into a separate 1.5 ml microfuge tube, and both tubes were stored at -80^{o}C.

Immediately after the cardiac bleed was conducted, the dead mouse was moved into a fumehood and pined down on a prepared workspace. Sterile surgical scissors were used to open a ventral incision from its abdomen, and a hypodermic needle was inserted into the heart to allow ice-cold PBS perfusion of the circulatory system to flush remaining blood.

Once the perfusion outflow was clear, kidneys, spleen, lungs, heart, spinal cord, and half the liver were harvested and placed into pre-labelled, sterile, screw-capped 1.5 ml microfuge tubes for immediate immersion in liquid nitrogen and long-term storage at -80^{o}C.

As shown in Figure 2.4.2, the mouse brain was halved along the midline, and one half was divided into five 2mm slices across its latitude, perpendicular to the initial cutting axis. Each slice was also placed into a 1.5 ml tube that was then immersed in LN2 and stored at -80^{o}C in the same manner.

A separate segment of the liver was also placed into a sterile 50 ml container containing 4% PFA fixative, along with the remaining half of the brain. Eyes were also removed and placed into a sterile 5 ml tube containing Davidson's fix. Both containers were stored at 4^{o}C. The Davidson's fix buffer was exchanged for 100% ethanol 24 hours after sample collection, and the PFA buffer was exchanged for sterile cold PBS 48 hours after sample collection. With the exception of L3 brain slices, samples collected were stored for future analysis outside the scope of this project.

Attribution: Mouse euthanasia was carried out by Dr Adeline Lau, and sample collection was carried out with assistance from Dr Adeline Lau.

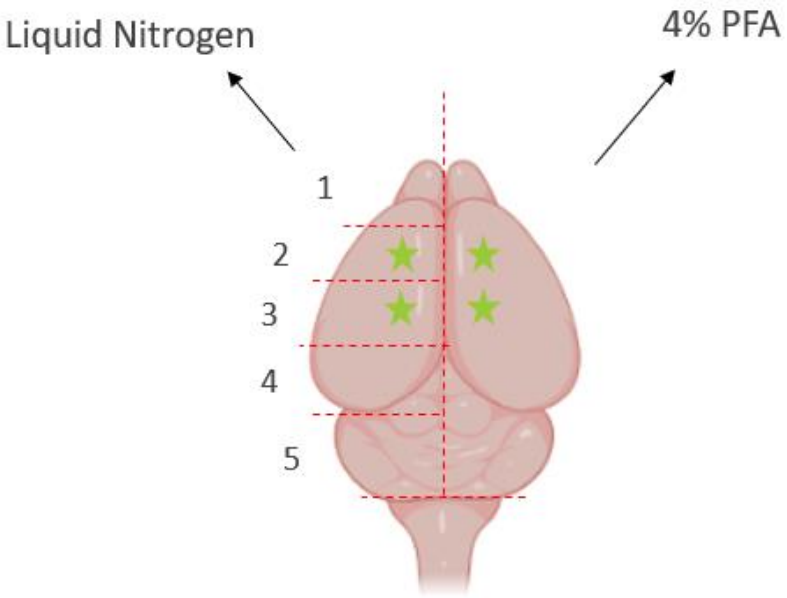

Figure 2.4.2: *Diagram of mouse brain dissection with sample slices numbered. Green stars denote approximate location of treatment injection sites. Mouse Brain image sourced from Biorender.com.*

2.4.1.4 Sample Genotyping for allele verification.

In preparation for genotyping of the mouse samples, the 40x custom Taqman SNP genotyping assay stock had the following probe and primer sequences added:

Forward Primer: 5'ACG CCC TCT GCT CTG TCT TC 3'

Reverse Primer: 5' GCG ATG GCA GTG TTG TTG TAT AC 3'

Probe WT: 5'VIC-TCA GCG **G**AT GAC GG-NFQ-MGB 3'

Probe Mutant: 5' FAM-TCA GCG **A**AT GAC GG-NFQ-MGB 3'

Stored ear samples were each combined with 100 µl prewarmed 10% Chelex-100 and vortexed thoroughly before being placed into a 100ºC heating block for 10 minutes. They were then vortexed again and heated for a further 10 minutes, before being centrifuged for 3 minutes at 13,000g using a Heraeus Biofuge-pico centrifuge to separate out cellular debris.

Total DNA content of the supernatant was analysed using a nanodrop 1000 spectrophotometer, and genotyping samples were made up to 80 µl volumes at a 2.5 ng/µl DNA concentration.

A genotyping mastermix was prepared using sterile water, Taqman Genotyping Mastermix, and primed 40x custom MPS assay at a ratio of 1.375 ul, 2.5 ul, and 0.125 ul respectively, per sample to be analysed.

1 µl of each sample was plated in the wells of a MicroAmp 96 well plate, and each well received 4 µl of the prepared mastermix before being sealed with an adhesive film and spun on a Axyspin mini plate centrifuge to ensure proper settling.

The plate was then run on a BioRad CFX Opus real time PCR system set to a volume of 5µl and a lid temp of 95ºC. Steps were as follows: 30 sec 60ºC, 10 mins 95ºC, then a repeated cycle of 15 sec 95ºC, 1 min plate read at 60ºC, for a total of 40 denaturation/annealing cycles.

Attribution: Sample genotyping was carried out with assistance from Mr Daniel Neumann.

2.4.2 Experiment 4: Preparation and Analysis of Harvested L3 Brain Slice Samples

2.4.2.1 Tissue Homogenisation

The L3 brain slice samples from the mouse cohort were removed from -80ºC storage and placed into Fast Prep-24 2ml lysing matrix D tubes containing 500µl 0.02 M Tris, 0.5 M NaCl buffer, pH7.4, stored on ice.

Samples were homogenised using a Precellys 24 tissue homogeniser set to 6500rpm, 2x 20 second bursts at 4^{o}C, and immediately placed onto ice afterwards.

2.4.2.2 Dialysis of homogenised samples for SGSH enzyme activity assay

100 µl of each homogenised sample was dialysed overnight in 2 L 0.2M sodium acetate at pH 6.5, 4^{o}C, through a 6-8 kD MWCO SpectraPor dialysis membrane. Samples were then retrieved from dialysis solution and sterile pipette was used to puncture the membrane and withdraw the sample for BCA testing and the SGSH enzyme assay.

A Thermo Fisher Scientific Micro-BCA protein assay kit was used to determine the protein concentration of the homogenised and dialysed mouse brain samples, using dilutions of its provided bovine serum albumin as standards on a clear, flat bottom 96 well microplate. The cell samples were plated in duplicate, with 15 µl sample to 85 µl Milli-Q water. 100 µl of the mixed BCA reagent was added to each well, and the plate was incubated for 2 hours at 37^{o}C before absorbance was read at 562 nm.

A BCA assay was performed as per the first paragraph of method 2.3.2.4, using the dialysed mouse brain samples. No sample was aliquoted for dry-down. The BCA data was used to determine the protein concentration of each dialysed sample for use in later enzyme activity calculations.

2.4.2.3 Determination of *SGSH* enzyme activity

10µl of each dialysed sample was combined with 20µl 2.2 mg/ml MU-αGLcNS in screw-capped Eppendorf tubes. Additionally, negative and positive controls were prepared using 10µl sodium acetate or 5µl sodium acetate mixed with 5µl purified rh*SGSH* respectively, combined with the same 20µl volume of 2.2 mg/ml MU-αGLcNS per control, in screw-capped Eppendorf tubes.

All tubes were capped, vortexed, and spun down briefly, before being incubated at 47^{o}C in a heating block for precisely 16 hours.

Samples were removed onto ice, and each received 6 µl Pi/Ci buffer and 10 µl α-glucosidase before being briefly vortexed and incubated 37^{o}C in a heating block for 24 hours.

Samples were removed onto ice, and each received 100 µl stop buffer, before being transferred to a clear, flat-bottomed 96 well microplate. Standards were prepared in duplicate using 10 µl of 4-MU standard diluted to various concentrations in Milli-Q water, combined

with 10µl sodium acetate, 20µl 2.2 mg/ml MU-αGLcNS, 6 µl Pi/Ci buffer, 10 µl α-glucosidase, and 100 µl stop buffer.

Fluorescence was measured a Spectramax iD5 plate reader at 355/460 nm, using a 1-second exposure, and recorded as fluorescence units. The enzyme activity rate for each sample, in picomoles per minute per milligram of protein, was determined using by comparing counts to a 4-methylumbelliferone standard curve and taking into account incubation time and sample protein content from the prior BCA assay.

2.4.2.4 Sample preparation for heparan sulfate assay

A BCA assay was performed as per method 2.3.2.4, using the remaining homogenized mouse brain samples. A total of 10 µg protein was aliquoted for dry-down.

2.4.2.5 Butanolysis assay of tissue heparan sulfate storage.

Butanolysis preparation and MS assay of dried down samples was carried out as per method 2.3.2.5, following established methodology (He et al. 2019).

Attribution: Liquid chromatography and mass spectrometry methods were carried out by Dr. Paul Trim and Dr. Marten Snel at SAHMRI, as per established methods (He *et al.* 2019).

2.5 Statistical Analysis:

Statistical analysis was performed via one-way ANOVA with Bonferroni post-hoc testing in GraphPad Prism.

2.6 Approvals:

IBC Approval No. #2020.03.2 ‘Intracerebral-parenchymal (ICP) and Intracerebral-ventricular (ICV) administration of genetic vector via modified synthetic liposomes – Exempt dealing’

IBC Approval No. #2022.15 ‘Non-viral gene therapy as a potential treatment for Sanfilippo syndrome’.

AEC Approval no. #4215-6 ‘Evaluation of a nanoparticle based therapy for Sanfilippo syndrome’.

Results:

3.1 Characterisation of liposome nanoparticles

3.1.1 Nanoparticle pDNA Encapsulation Ratio

As per the methods in Section 2.2.3, 4 ng/ml pDNA in citrate buffer was mixed with a custom lipid formulation to initiate encapsulation. The resulting nanoparticle preparations were then evaluated using a PicoGreen assay, as per the methods in Section 2.3.5.

The first nanoparticle batch used for cell work (Experiments 1, 2, and 3) had an initial DNA concentration of 12.5 ng/µl, and after liposome disruption with Triton-X100, it had a DNA concentration of 102.7 ng/µl, indicating an encapsulation ratio of 87.8%.

The second nanoparticle batch used for mouse work (Experiment 4) had an initial DNA concentration of 21 ng/µl, and after liposome disruption with Triton-X100, it had a DNA concentration of 108.1 ng/µl, indicating an encapsulation ratio of 80.6%.

3.1.2 Nanoparticle Sizing and Size Distribution

When measured using the dynamic light scattering function of a Malvern Zetasizer™, the first nanoparticle batch was found to have an average particle size of 125.8 nm with a standard deviation of 0.7 nm, as shown in Figure 3.1. The second nanoparticle batch was found to have an average particle size of 105.4 nm with a standard deviation of 4.74 nm, as shown in Figure 3.2.

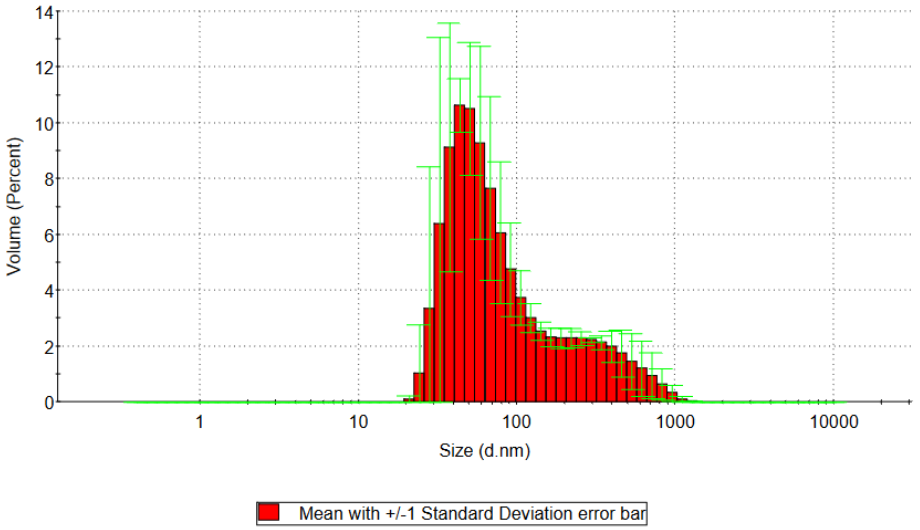

Figure 3.1: *Size distribution of first-batch liposome nanoparticles in sterile saline solution as measured using a Malvern Zetasizer™ via dynamic light scattering. Average size of 125 nm with a standard deviation of 0.7 nm.*

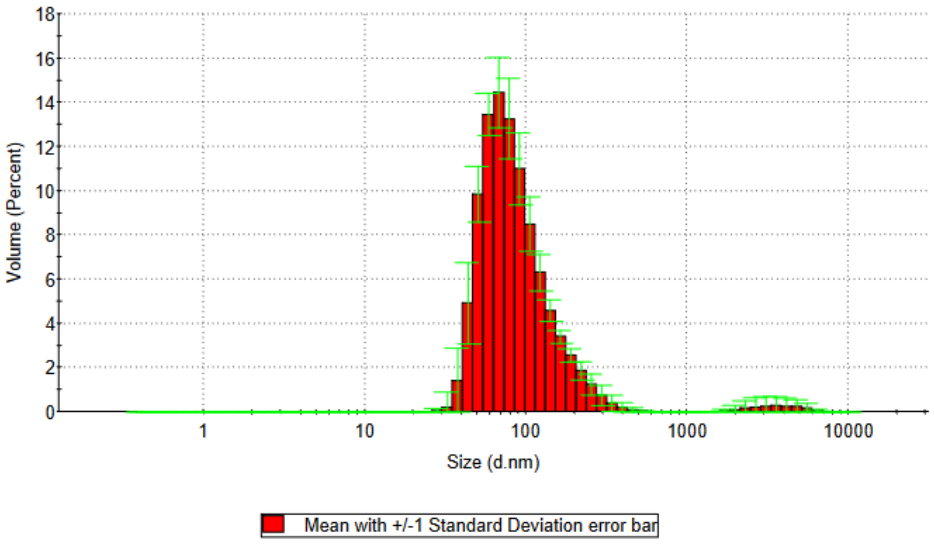

Figure 3.2: *Size distribution of second-batch liposome nanoparticles in sterile saline solution as measured using a Malvern Zetasizer™ via dynamic light scattering. Average size of 105 nm with a standard deviation of 4.7 nm.*

3.2 Results of in vitro human fibroblast experiments

3.2.1 Cellular heparan sulfate

As per the methods in Section 2.3.2, fibroblasts were treated with unencapsulated DNA plasmids or designed nanoparticles containing the same plasmids, at doses of 0.5, 1, or 2 picograms per cell, allowed to grow for 4 days (after observed toxicity effects precluded initial plans of a 7-day duration) and then processed for analysis of heparan sulfate levels.

Disaccharide / Internal Standard (IS) peak area ratios from triplicate wells were analysed using one-way ANOVA with Bonferroni post-hoc testing via GraphPad Prism. While prior work has established that the MPS-IIIA model fibroblasts have elevated heparan sulfate levels compared to the wildtype line used, this experiment did not have the statistical power to show a significant difference between the two, with a P-value >0.9999.

As seen in Figure 3.3, the heparan sulfate levels of control MPS-IIIA fibroblasts did not statistically differ from wildtype controls. MPS-IIIA fibroblasts treated with 0.5 or 1 pg/cell encapsulated nanoparticles visually indicated elevated heparan sulfate levels, however statistical tests did not show any significant difference between MPS-IIIA control treatment and any DNA or nanoparticle treatment. However, there was a statistically significant difference between the 0.5 and 2 picogram/cell nanoparticle treatments, at a P-value of 0.0186.

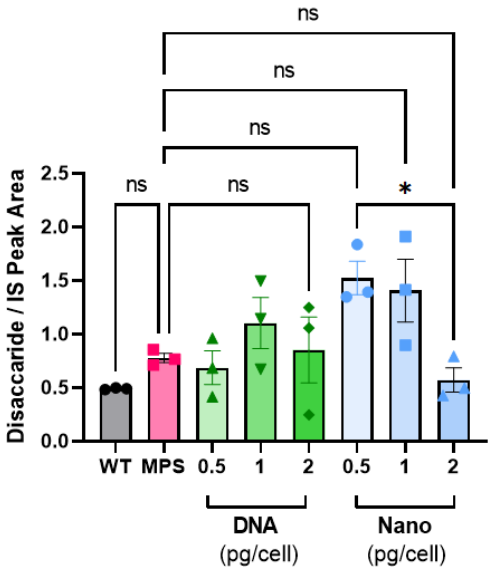

Figure 3.3: *Relative heparan sulfate of MPS-IIIA disease model human fibroblasts following 4-day treatment with nanoparticles or naked DNA plasmids at 0.5, 1, or 2 picograms per cell, along with PBS-treated vehicle controls (N=3 per treatment). Data shown as mean ± SEM from triplicate wells. Statistical analysis performed via one-way ANOVA with Bonferroni post-hoc testing in GraphPad Prism.*

3.2.3 Cellular lysosomal enlargement

Due to the inconclusiveness of the heparan sulfate data, lysosomal enlargement was investigated as an alternative indicator of MPS-IIIA disease severity that could be quickly pursued using existing material stocks, to gain a better picture of how nanoparticle treatment was impacting the disease profile.

As per the methods in Section 2.3.3, fibroblasts were treated with designed nanoparticles containing *SGSH*-encoding plasmids, at doses of 2 or 4 picograms per cell, allowed to grow for 4 days, and then processed for analysis of lysosomal size based on the signal ratio of lysotracker and nuclear stain. Statistical analysis was performed using one-way ANOVA with Bonferroni post-hoc testing via GraphPad Prism.

As shown in Figure 3.4, the MPS-IIIA control treatment had significantly higher lysotracker signal per cell than the wildtype control treatment, and MPS-IIIA cells at both nanoparticle treatment concentrations showed significantly higher lysosomal storage compared to the MPS-IIIA control, with P-values <0.0001. Additionally, the 4 picogram/cell nanoparticle treatment showed a statistically significant decrease compared to the 2 picogram/cell nanoparticle treatment, with a P-value of 0.0182.

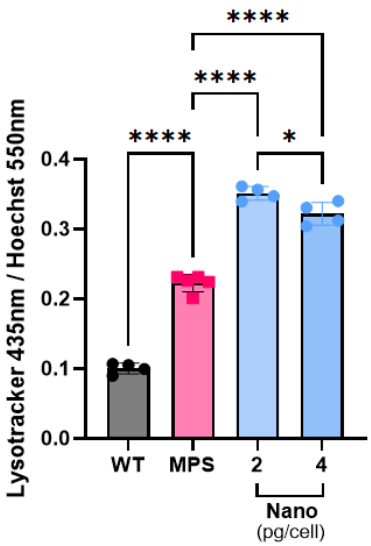

Figure 3.4: *Lysosomal storage per cell of MPS-IIIA disease model human fibroblasts following 4-day treatment with nanoparticles at 2 or 4 picograms per cell, along with PBS-treated vehicle controls. Data shown as mean ± SEM from 4 wells per treatment, or 5 for MPS control. Statistical analysis performed via one-way ANOVA with Bonferroni post-hoc testing in GraphPad Prism.*

3.2.5 Cellular autophagic activity

In light of the unusual lysosomal size data, an alternative staining method that focused on autophagic markers was pursued. Ideally, it would provide an alternative perspective of how nanoparticle treatment was impacting the autophagic activity within the cells.

As per the methods in Section 2.3.4, fibroblasts were treated with unencapsulated DNA *SGSH*-coding plasmids or designed nanoparticles containing the same plasmids, at doses of 2 or 4 picograms per cell, allowed to grow for 4 days, and then processed for analysis of lysosomal size based on the signal of an anti-p62 immunofluorescence marker normalised to the number of nuclei. Statistical analysis was performed using one-way ANOVA with Bonferroni post-hoc testing via GraphPad Prism.

As shown in Figure 3.5, the wildtype control showed significantly higher signal than the MPS-IIIA control, with a P-value of <0.0001. Both DNA treatments and the 2 pg/cell nanoparticle treatment were not statistically different from the MPA-IIIA control.

Notably, the 4 pg/cell nanoparticle treatment showed significantly higher signal than the MPA-IIIA control by a slim margin, with a P-value of 0.0009, and was not statistically different from the wildtype control, with a P-value of >0.9999.

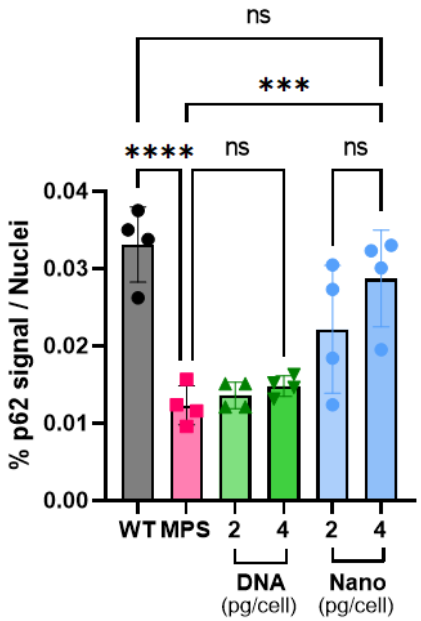

Figure 3.5: *p62 antibody signal per cell of MPS-IIIA disease model human fibroblasts following 4-day treatment with nanoparticles or naked DNA plasmids at 2 or 4 picograms per cell, along with PBS-treated vehicle controls. Data shown as mean ± SEM from 4 wells per treatment. Statistical analysis performed via one-way ANOVA with Bonferroni post-hoc testing in GraphPad Prism.*

3.3 Results of in vivo mouse experiments

3.3.1 Mouse weight trends post-surgery

After mice were treated with unencapsulated DNA, nanoparticles, or PBS vehicle solutions via intercranial injection, their weight was closely monitored over 4 weeks before they were euthanized. One mouse from the nanoparticle treatment group was humanely euthanized on day 3 after surgery when a sustained tremor was observed, however post-mortem analysis did not show any abnormalities concerning the teeth, brain, or organs.

As shown in Figure 3.6, all treatment groups gained weight over the observational period with the nanoparticle treatment group gaining the most weight relative to starting bodyweight.

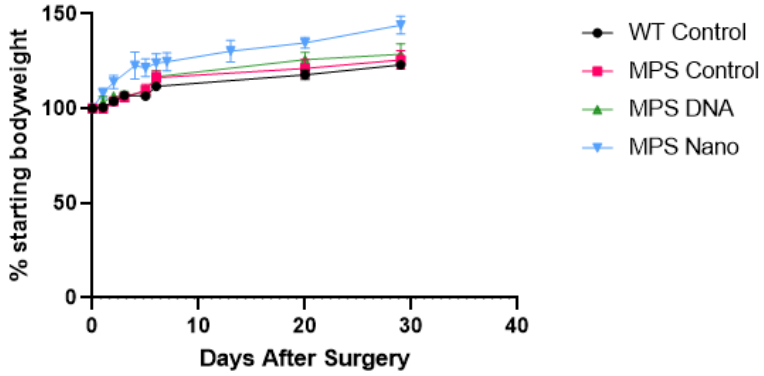

Figure 3.6: *Average mouse weight by treatment group as a percentage of starting bodyweight. Mice received surgery at 6 weeks of age and were euthanized 4 weeks post-surgery. Data shown as mean ± SEM. Total 5 mice per group, or 4 mice for Nanoparticle treatment group.*

3.3.3 *SGSH* enzyme activity in homogenised L3 brain slices

As per the methods in Section 2.4.2 (.1-.3), L3 brain slices from the euthanized mouse treatment groups were homogenized, dialysed, and assayed for sulfamidase activity. Genotyping confirmed accuracy of WT and MPS labelling of samples in cohort. Statistical analysis was performed using one-way ANOVA with Bonferroni post-hoc testing via GraphPad Prism.

As shown in Figure 3.7, all three of the MPS treatment groups did not show any detectable enzyme activity. Due to this, the enzyme activity of the wildtype control samples was significantly higher than all other treatment groups, with a P-value <0.0001 in all cases. Additionally, there was no significant differences between any of the MPS-IIIA treatment groups, with P-values >0.9999 in all cases.

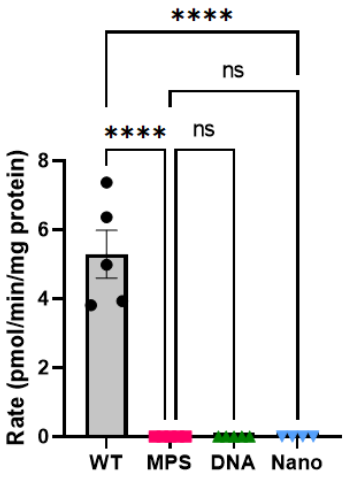

Figure 3.7: *Sulfamidase activity of homogenized L3 mouse brain slice samples in picomoles of substrate processed per minute, per mg of protein in the sample. Mice underwent 30-days growth after intraparenchymal treatment with plasmid-carrying nanoparticles or naked DNA plasmids, both at $5x10^{12}$ plasmid copies per kilogram of bodyweight, along with PBS-treated vehicle controls. Data shown as mean ± SEM from 5 mouse samples per treatment, or 4 for the nanoparticle treatment group. Statistical analysis performed via one-way ANOVA with Bonferroni post-hoc testing in GraphPad Prism.*

3.3.5 Mouse heparan sulfate levels in homogenised L3 brain slices

As per the methods in Section 2.4.2 (.1, .4, .5), L3 brain slices from the euthanized mouse treatment groups were homogenized, dried down, digested, and assayed for total heparan sulfate content. Genotyping confirmed accuracy of WT and MPS labelling of samples in cohort. Statistical analysis was performed using one-way ANOVA with Bonferroni post-hoc testing via GraphPad Prism.

As shown in Figure 3.8, all MPS-IIIA treatment groups had significantly higher heparan sulfate levels compared to the wildtype control treatment, with P-values <0.0001. Additionally, all MPS-IIIA treatment groups had no statistically significant differences in heparan sulfate content, with P-values >0.9999.

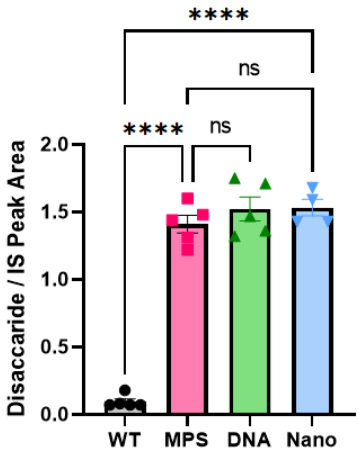

Figure 3.8: *Relative heparan sulfate storage of homogenized L3 mouse brain slice samples. Mice underwent 30-days growth after intraparenchymal treatment with plasmid-carrying nanoparticles or naked DNA plasmids, both at 5x10^{12} plasmid copies per kilogram of bodyweight, along with PBS-treated vehicle controls. Data shown as mean ± SEM from 5 mouse samples per treatment, or 4 for the nanoparticle treatment group. Statistical analysis performed via one-way ANOVA with Bonferroni post-hoc testing in GraphPad Prism.*

Discussion:

4.1 Nanoparticle characterisation

In terms of encapsulation, a higher percentage is more desirable as it indicates that more of the pDNA plasmid copies used in the nanoparticle preparation methods have been successfully packaged for delivery via the nanoparticles. A low encapsulation ratio would require greater volumes to be delivered for the same level of gene expression, resulting in more invasiveness *in vivo* and greater quantities of lipids to be cleared by cellular processes.

For this therapeutic approach, it is critical that the nanoparticles are small enough to effectively travel throughout the brain. Literature indicates that nanoparticle diameter of approximately 100 nm is preferred for longer-term circulation, and a size of approximately 160 nm is preferable for cellular uptake (Zu & Gao 2021).

The nanoparticle sizing data shown in Figures 3.1 and 3.2 appears to approximate a normal distribution, with the addition of a significant 'tail' comprised of larger particles within the tested aliquots, likely representing aggregation of excess lipids or improperly formed nanoparticles. Since further filtration steps were conducted after those aliquots were taken for size analysis, this is unlikely to have an experimental effect. This hypothesis is supported by the fact that the 'tail' is less prominent in the second batch, undertaken after experience has been gained with the preparation process.

Overall, the characteristics of the produced nanoparticles match up to the guideline ranges indicated in the literature and were similar or better than those obtained by previous batches made by the CDRG lab and collaborators. For example, the nanoparticle batches used in the prior work related to GFP had encapsulation ratios of 83.9% and 78.5%, while these batches had encapsulation ratios of 87.8% and 80.6% (*Childhood Dementia Research Group, unpublished data*). Therefore, the particles were deemed suitable for experimental use.

Additional tests could theoretically have been run using PCR gels to determine the integrity of the DNA after liposome disruption. Observing degraded fragments in the gel would not be conclusive, as DNA damage may occur due to the disruption process, but observation of intact DNA would verify that the encapsulated DNA was not degraded by the encapsulation process.

4.2 Cellular heparan sulfate

Based on existing literature, it was expected that the MPS-IIIA control group would have significantly elevated heparan sulfate levels compared to the wildtype control group, due to accumulation of the substrate being the primary result of the disorder's impaired enzyme function (Sanfilippo *et al.* 1963).

As such, the control results initially appeared as expected, with the MPS-IIIA cell line visually indicated to have higher heparan sulfate levels compared to the wildtype cell line. However, this increase proved to not be statistically significant, likely due to variability induced by operator inexperience, compounded by the limited replicates per treatment group (n=3), resulting in weak statistical power. Due to such a control issue, the experiment cannot meaningfully support or contradict the hypothesis without additional data.

Prior experiments using the same cell lines have shown a statistical difference, however direct comparison of data is not possible due to heparan sulfate levels being expressed as a signal ratio within the samples contained on the specific treatment plate, instead of a value derived from standards of known concentration. Such standards have been used in previous projects, but where unavailable at the time of this experiment.

DNA treatments were hypothesized to minimally lower heparan sulfate levels in a stepwise, dose respondent fashion, but due to not having a proper delivery vector to ensure a high transduction efficiency and protect from endonucleases (Ginn *et al*. 2018), this effect being non-significant was also considered probable. In keeping with this, the data did not show any significant difference between the DNA-treated MPS-IIIA treatment groups and the MPS-IIIA control group.

Nanoparticle treatments were hypothesized to lower heparan sulfate levels in a stepwise, dose respondent fashion. The first part of this hypothesis was not supported, as the nanoparticle treatments did not induce a statistically significant corrective effect, however there was a statistically significant difference between the 0.5 pg/cell and 2 pg/cell nanoparticle treatments, potentially supporting a dose-responsive correction toward wildtype levels of heparan sulfate.

Overall, the experiment lacked statistical power and was not conclusive. Repetition of the experiment with greater technical experience and precision, or larger treatment groups, may provide more conclusive data.

4.3 Cellular lysosome size

Progressive accumulation of undegraded heparan sulfate in cellular lysosomes is characteristic of Sanfilippo syndrome and results in increased size of lysosomal compartments (Walkley 2004, Beneto *et al.* 2020). Due to this, lysosomal size serves as an alternative indicator of potential therapeutic effectiveness, and experimental materials were available to investigate this marker quickly and efficiently.

Control results were as expected, with the MPS-IIIA control group having higher significantly lysosomal storage compared to the wildtype control group.

Nanoparticle treatments were hypothesized to reduce lysosomal storage via inducing expression of sulfamidase and the enzyme's subsequent breakdown of accumulated heparan sulfate in cellular lysosomes. This hypothesis was not supported by the obtained data, with a significant increase in lysosomal storage observed instead.

Straightforward failure to induce expression would not produce the increase observed, therefore, it is likely that aggerated products from the nanoparticles themselves were contributing to lysosomal loading while the cells process the lipid residues, as existing literature indicates can occur (Stern *et al.* 2012, Uzhytchak *et al.* 2023).

Additionally, there was a statistically significant decrease in lysosomal size between the 2 and 4 pg/cell nanoparticle treatments. This seemingly dose-responsive reduction between the nanoparticle treatments potentially indicates the expected therapeutic effect occurring, even if lipid lysosomal loading is increasing lysosomal storage overall and 'masking' the corrective effect. Since the lipids should be degraded over time by normal cellular functions, repeating the experiment with a longer experimental duration may potentially allow the treated cells to clear any lysosomal loading and give a better indication of treatment effectiveness.

4.4 Cellular autophagic activity

Another biomarker for Sanfilippo syndrome is p62, a protein encoded by the *SQMST1* gene that is positively related to autophagosome activity and specific autophagy. (Kumar *et al.* 2022).

Due to the upregulation of p62 in situations where cellular protein degradation is impaired, it was hypothesized that the MPS-IIIA control treatment would show significantly elevated p62 signal compared to the wildtype control group. However, the data showed the reverse trend, with the wildtype control having significantly higher p62 signal per cell.

The unencapsulated DNA treatments did not show a significant difference to the MPS-IIIA control group, however the nanoparticle treatments did show both a significant difference to the MPS-IIIA control group, and no significant difference to the wildtype control group.

While this would normally indicate a correction toward the wildtype phenotype, and thus a therapeutic effect, the increase in autophagy-linked p62 signal does not match established behaviours for the biomarker itself (Kumar *et al.* 2022), or prior studies in MPS-IIIA models using p62 immunostaining (Winner *et al.* 2016).

Additionally, there is a high likelihood of flawed data due to errors in methodology or experimental design. Specifically, higher cell mortality was observed in edge and corner wells during the 4-day growth period after treatment, and the observed p62 signal trend across the treatment groups is highest in the treatments that were outermost on the growth plate, and lowest in the treatments that were centremost on the growth plate (as seen by cross-referencing table 5 and Figure 3.5). This implicates oxidative stress or media evaporation impacting the data.

As such, the experiment could be repeated with randomized well locations and precautions against evaporative stresses in order to control for that potential. Analysis of liposomes without encapsulated DNA as a control treatment is not possible due to the charge-related liposome formulation process.

4.5 Mouse weight trends

Mouse weight trends were positive and did not show any notable differences between the wildtype control, MPS-IIIA control, and DNA treatment groups. The nanoparticle treatment group did show a greater increase in relative bodyweight post-treatment; however, this was due to a lower mean bodyweight at the time of surgery, and all treatment groups had equivalent bodyweights at the time of euthanasia.

4.6 *SGSH* enzyme activity in mouse brain samples

Impaired *SGSH* enzyme activity, or more specifically sulfamidase activity, is a clear and specific biomarker of MPS-IIIA disease pathology (Whyte *et al.* 2015). As such, it was expected that the wildtype control would exhibit significantly higher enzyme activity than the MPS-IIIA control group, that was expected to show extremely minimal or no enzyme activity. This hypothesis was supported, with the MPS-IIIA control showing no detectable enzyme activity and the wildtype control showing significant enzyme activity.

The DNA treatments were expected to have minimal effect, as while some transduction should occur, it was likely to be below the sensitivity of the assay. The data showed no detectable enzyme activity in the DNA treatments, and thus no significant difference between the DNA treatments and the MPS-IIIA controls.

There was no clear hypothesis as to the expected enzyme activity of the nanoparticle treatments, but if they did show activity, it would be a strong indicator of a therapeutic effect. However, the data showed no detectable enzyme activity, and thus no significant difference between the nanoparticle treatments and the MPS-IIIA controls.

If another *in vivo* experiment was conducted, a longer post-treatment growth period may allow greater *SGSH* expression and a higher sulfamidase activity in the brain samples that could prove detectable. Alternatively, there may have been technical errors due to the complexity and long duration of the enzyme activity assay methodology.

4.7 Heparan sulfate levels of mouse brain samples

As previously noted, cellular accumulation of heparan sulfate is a primary indicator of MPS-IIIA disease pathology (Beneto *et al.* 2020, Sanfilippo et al. 1963).

Based on this, it was hypothesized that the MPS-IIIA control group would have significantly elevated heparan sulfate levels compared to the wildtype control group, the DNA treatment group may show minor corrective effects but are likely to not significantly differ from the MPS-IIIA control group, and that the nanoparticle control group would show a correction effect with significant change from the MPS-IIIA control group.

The data showed a significant difference between the MPS-IIIA control group and the wildtype control group, with the samples from the disease-model mice having elevated heparan sulfate as expected. However, both the DNA and nanoparticle treatment groups did not significantly differ from the MPS-IIIA control group.

The lack of notable reduction in heparan sulfate after treatment may indicate a need for longer post-treatment growth periods, in order to allow for greater *SGSH* expression and corrective effect. Additionally, histological analysis of brain tissues has been used to determine therapeutic effect in similar studies with AAV vectors, and may be a more sensitive method that is applicable here (Winner *et al.* 2016), however initial LIMP2 staining and analysis has not indicated an observable change, as shown in Appendix C below.

4.8 Summary of progress and future avenues

Most of the experiments undertaken have been inconclusive, and while the transfection capability of the nanoparticle formulation and the SGSH expression of the plasmid were established via prior work, the ability of the combined therapy to induce corrective SGSH expression still needs to be shown. As such, experiments focused on showing DNA integrity after encapsulation, delivery of the DNA into cells, and subsequent expression of that DNA need to be devised, potentially involving DNA PCR or alternative immunohistochemical targets less related to autophagy and more specific to SGSH.

Due to the limited 4-day duration of the in-vitro experiments, repetition of the experiments using longer experimental durations (7-10 days) will be desirable in order to better confirm the data trends and determine if sustained gene expression and metabolization of potential lipid residues shows a corrective effect. Plate randomisation could also be adopted to control for observed toxicity effects at plate edges, and further investigation into potential lysosomal loading with lipid residues will be important to understand the performance and limitations of lipid nanoparticle vectors as a therapeutic approach.

Additionally, modifications and optimisations could be made to the nanoparticle formulation in order to refine encapsulation efficiency, with the aim to improve transportation efficacy *in vivo*, transduction efficiency, and to reduce potential toxicity or autophagic disruption by reducing the overall volume of delivered lipids.

References:

Albertson, C., Kulkarni, J., Witzigman, D., Lind, M., Petersson, K., Simonsen, J. (2022) The role of lipid components in lipid nanoparticles for vaccines and gene therapy, *Advanced Drug Delivery Reviews*, 188(1), pp. 1-17. https://doi.org/10.1016/j.addr.2022.114416

Andrade, F., Aldamiz-Echevarría, L., Llarena, M., Couce, M. (2015) Sanfilippo syndrome: Overall Review, *Pediatrics International*, 57(3), pp. 331-338. https://doi.org/10.1111/ped.12636

Anthony, F. (2015) Sanfilippo syndrome: Causes, consequences, and treatments, *The Application of Clinical Genetics*, 8(1), pp. 269-281. http://doi.org/10.2147/TACG.S57672

Australian Institute of Health and Welfare. (2021) Dementia in Australia 2021: Summary Report, *Australian Institute of Health and Welfare*, Canberra. <https://www.aihw.gov.au/reports/dementia/dementia-in-australia-2021-summary/overview>

Beneto, N., Vilageliu, L., Grinberg, D., Canals, I. (2020) Sanfilippo Syndrome: Molecular Basis, Disease Models and Therapeutic Approaches, *International Journal of Molecular Sciences*, 21(21), pp. 1-20. https://doi.org/10.3390/ijms21217819

Bulcha, J., Wang, Y., Ma, H., Tai, P, Gao, G. (2021) Viral vector platforms within the gene therapy landscape, *Signal Transduction and Targeted Therapy*, 6(53), pp. 1-24. https://doi.org/10.1038/s41392-021-00487-6

Cawley, A., Gliddon, B., Auclair, D., Brodie, S., Hirte, C., King, B., Fuller, M., Hemsley, K., Hopwood, J. (2006) Characterization of a C57BL/6 congenic mouse strain of mucopolysaccharidosis type IIIA, *Brain Research*, 1104(1), pp. 1-17. https://doi.org/10.1016/j.brainres.2006.05.079

Chin, S., Fuller, M. (2022) Prevalence of lysosomal storage disorders in Australia from 2009 to 2020, *The Lancet Regional Health - Western Pacific*, 19(1), https://doi.org/10.1016/j.lanwpc.2021.100344

Clarke, D., Pearse, Y., Kan, S., Le, S., Sanghez, V., Cooper, J., Dickson, P., Lacvino, M. (2018) Genetically Corrected iPSC-Derived Neural Stem Cell Grafts Deliver Enzyme Replacement to Affect CNS Disease in Sanfilippo B Mice, *Molecular Therapy - Methods and Clinical Development*, 10(1), pp. 113-127. https://doi.org/10.1016/j.omtm.2018.06.005

Concolino, D., Deodato, F., Parini, R. (2018) Enzyme replacement therapy: efficacy and limitations, *Italian Journal of Pediatrics*, 44(2), pp. 117-126. https://doi.org/10.1186%2Fs13052-018-0562-1

Cure Sanfilippo Foundation. (2019) What is Sanfilippo syndrome? Child progression guideline. Viewed 3 February 2023.

Diaz, J., Castillo, J., Rodriguez-Lopez, E., Almeciga-Diaz, C. (2020) Advances in the Development of Pharmacological Chaperones for the Mucopolysaccharidoses, *International Journal of Molecular Sciences*, 21(1), pp. 1-19. https://doi.org/10.3390/ijms21010232

Gill, D., Pringle, I., Hyde, S. (2009) Progress and Prospects: The design and production of plasmid vectors, *Gene Therapy*, 16(1), pp. 165-171.

Ginn, S., Amaya, A., Alexander, I., Edelstein, M., Abedi, M. (2018) Gene therapy clinical trials worldwide to 2017: An update, *The Journal of Gene Medicine*, 20(5), pp. 1-6. https://doi.org/10.1002/jgm.3015

Global Burden of Disease Collaborators. (2021) Global mortality from dementia: Application of a new method and results from the Global Burden of Disease Study 2019. *Alzheimer's Association*, 7(1), pp. 1-28. https://doi.org/10.1002/trc2.12200

He, Q., Trim, P., Lau, A., King, B., Hopwood, J., Hemsley, K., Snel, M., Ferro, V. (2019) Synthetic Disaccharide Standards Enable Quantitative Analysis of Stored Heparan Sulfate in MPS IIIA Murine Brain Regions, *ACS Chemical Neuroscience*, 10(8), pp.3847-3858. https://doi.org/10.1021/acschemneuro.9b00328

Hendriks, S., Peetoom, K., Bakker, C., Koopmans, R., Flier, W., Papma, J., Verhey, F., Young-Onset Dementia Study Group. (2022) Global incidence of young-onset dementia: A systematic review and meta-analysis, *Alzheimer's Association*, online preview. https://doi.org/10.1002/alz.12695

Heybrock, S., Kanerva, K., Meng, Y., Ing, C., Liang, A., Xiong, Z., Weng, X., Kim, Y., Collins, R., Trimble, W., Pomes, R., Pirve, G., Annaert, W., Schwake, M., Heeren, J., Lullman-Rauch, R., Grinstein, S., Ikonen, E., Saftig, P., Neculai, D. (2019) Lysosomal integral membrane protein-2 (LIMP-2/SCARB2) is involved in lysosomal cholesterol export, *Nature Communications*, 10(3521), pp. 1-12. https://doi.org/10.1038/s41467-019-11425-0

Hocquemiller, M., Hemsley, K., Douglass, M., Tamang, S., Neumann, D., King, B., Beard, H., Trim, P., Winner, L., Lau, A., Snel, M., Gomila, C., Ausseil, J., Mei, X., Geirsh, L., Plavsic, M., Laufer, R. (2020) AAVrh10 Vector Corrects Disease Pathology in MPS IIIA Mice and Archives Widespread Distribution of SGSH in Large Animal Brains, *Molecular Therapy - Methods and Clinical Development*, 17(1), pp. 174-187. https://doi.org/10.1016/j.omtm.2019.12.001

James, B., Bennet, A. (2021) Causes and Patterns of Dementia: An Update in the Era of Redefining Alzheimer's Disease, *Annual Review of Public Health*, 40(1), pp. 65-84. https://doi.org/10.1146/annurev-publhealth-040218-043758

Karpova, E., Voznyi, Y., Keulmans, J., Hoogeveen, A., Winchester, B., Tsvetkova, I., Diggelen, O. (1995) A fluorimetric enzyme assay for the diagnosis of sanfilippo disease type A (MPS IIIA), *Journal of Inherited Metabolic Disease*, 19(3), pp. 278-285. https://doi.org/10.1007/BF01799255

Kauffman, K., Dorkin, R., Yang, J., Heartlein, M., DeRosa, F., Mir, F., Fenton, O., Anserson, D. (2015) Optimization of Lipid Nanoparticle Formulations for mRNA Delivery in Vivo with Fractional Factorial and Definitive Screening Designs, *Nano Letters*, 15(11), pp. 7300-7306. https://doi.org/10.1021/acs.nanolett.5b02497

Khon, A., Grigull, L., Moulin, M., Kabisch, S., Ammer, L., Rudolph, C., Muschol, N. (2020) Hematopoietic stem cell transplantation in mucopolysaccharidosis type IIIA: A case description and comparison with a genotype-matched control group, *Molecular Genetics and Metabolism Reports*, 23(1), pp. 1-6. https://doi.org/10.1016/j.ymgmr.2020.100578

Kong, W., Wu, S., Zhang, J., Lu, C., Ding, Y., Meng, Y. (2021) Global epidemiology of mucopolysaccaridosis type III (Sanfilippo syndrome): an updated systematic review and meta-analysis, *Journal of Paediatric Endocrinology and Metabolism*, 34(10), pp. 1225-1235. https://doi.org/10.1515/jpem-2020-0742

Kong, W., Yao, Y., Zhang, J., Lu, C., Ding, Y., Meng, Y. (2020) Update of treatment for mucopolysaccharidosis type III (sanfilippo syndrome), *European Journal of Pharmacology*, 888(1), pp. 1-7. https://doi.org/10.1016/j.ejphar.2020.173562

Kumar, A., Mills, J., Lapierre, L. (2022) Selective Autophagy Receptor p62/SQSTM1, a Pivotal Player in Stress and Aging, *Frontiers in Cell and Developmental Biology*, 10(1), pp. 1-11. https://doi.org/10.3389/fcell.2022.793328

Laporte, L., Rea, J., Shea, L. (2006) Design of modular non-viral gene therapy vectors, *Biomaterials*, 27(7), pp. 947-954. https://doi.org/10.1016/j.biomaterials.2005.09.036

Lavery, C., Hendriksz, C., Jones, S. (2017) Mortality in Patients with Sanfilippo Syndrome, *Orphanet Journal of Rare Diseases*, 12(168), pp. 2-7 https://doi:10.1186/s13023-017-0717-y

McIntosh, N., Berguig, G., Karim, O., Cortesio, C., Angelis, R., Khan, A., Gold, D., Maga, J., Bhat, V. (2021) Comprehensive characterization and quantification of adeno associated vectors by size exclusion chromatography and multi angle light scattering, *Nature Scientific Reports*, 11(3012), pp. 1-12. https://doi.org/10.1038/s41598-021-82599-1

Meikle, P., Hopwood, J., Clauge, A., Carey, W. (1999) Prevalence of Lysosomal Storage Disorders, *Journal of the American Medical Association*, 281(3), pp. 249-254. https://doi:10.1001/jama.281.3.249

Muenzer, J. (2011) Overview of the mucopolysaccharidoses, *Rheumatology*, 50(5), pp. 4-12. https://doi.org/10.1093/rheumatology/ker394

Parenti, G., Medina, D., Ballabio, A. (2021) The rapidly evolving view of lysosomal storage disorders, *EMBO Molecular Medicine*, 13(2), pp. 1-21. https://doi.org/10.15252/emmm.202012836

Penon-Portmann, M., Blair, D., Harmatz, P. (2023) Current and new therapies for mucopolysaccharidoses, *Pediatrics and Neonatology*, 64(1), pp. 10-17. https://doi.org/10.1016/j.pedneo.2022.10.001

Piotrowska, E., Jakobkiewicz-Banecka, J., Baranska, S., Tylki-Szymanska, A., Czartoryska, B., Wegrzyn, A., Wegrzyn, G. (2006) Genistein-mediated inhibition of glycosaminoglycan synthesis as a basis for gene expression-targeted isoflavone therapy for mucopolysaccharidoses, *European Journal of Human Genetics*, 14(1), pp. 846-852.

Rasko, J., Bashirians, G., Petropoulos, C., Wrin, T., Paliwal, Y., Somanathan, S., Casey, M., Pereira, C., Winburn, I., Chhabra, A. (2022) Global Seroprevalence of Neutralizing Antibodies Against Adeno-Associated Virus (AAV) Serotypes of Relevance to Gene Therapy, *Blood*, 140(1), pp. 10668-10670. https://doi.org/10.1182/blood-2022-158305

Robinson, A., Zhao, G., Rathjen, J., Rathjen, P., Hutchinson, R., Eyre, H., Hemsley, K., Hopwood, J. (2010) Embryonic Stem Cell-Derived Glial Precursors as a Vehicle for Sulfamidase Production in the MPS-IIIA Mouse Brain, *Cell Transplantation*, 19(1), pp. 985-998. https://doi.org/10.3727/096368910X498944

Ruijter, J., Valstar, M., Narajczyk, M., Wegrzyn, G., Kulik, W., Ijlst, L., Wagemans, T., Van der wal, W., Wijburg, F. (2011) Genistein in Sanfilippo disease: A randomized controlled crossover trial, *Annals of Neurology*, 71(1), pp. 110-120. https://doi.org/10.1002/ana.22643

Sanfilippo Children's Foundation. (2019) What is Sanfilippo? Sanfilippo Fact Sheet: disease family diagram. Viewed 9 February 2023.

Sanfilippo, S., Podosin, R., Langer, L., Good R. (1963) Mental retardation associated with acid mucopolysaccharidu ria (heparin sulfate type), *The Journal of Pediatrics*, 63(4), pp. 837-838. https://doi.org/10.1016/S0022-3476(63)80279-6

Schreck, K., Knapp, L. (2022) MPS-IIIA or Autism Spectrum Disorder?: Discrimination and Treatment, *Review Journal of Autism and Developmental Disorders*, 1(1), pp.1-8. https://doi.org/10.1007/s40489-021-00298-z

Shirley, J., Jong, Y., Terhorst, C., Herzog, R. (2020) Immune Responses to Viral Gene Therapy Vectors, *Molecular Therapy*, 28(3), pp. 709-722. https://doi.org/10.1016/j.ymthe.2020.01.001

Sidhu, N., Schreiber, K., Propper, K., Becker, S., Uson, I., Scheldrick, G., Gartner, J., Kratzner, R., Steinfield, R. (2014) Structure of sulfamidase provides insight into the molecular pathology of mucopolysaccharidosis IIIA, *Acta Crystallographica D Biological Crystallography*, 70(1), pp. 1321-1335. https://doi.org/10.1107%2FS1399004714002739

Stern, S., Adiseshaiah, P., Crist, R. (2012) Autophagy and lysosomal dysfunction as emerging mechanisms of nanomaterial toxicity, *Particle and Fibre Toxicology*, 9(20), pp. 1-15. https://doi.org/10.1186/1743-8977-9-20

Tomsen-Melero, J., Merlo-Mas, J, Carreno, A., Sala, S., Cordoba, A., Veciana, J., Gonzalez-Mira, E., Ventosa, N. (2022) Liposomal formulations for treating lysosomal storage disorders, *Advanced Drug Delivery Reviews*, 190(1), pp. 2-23. https://doi.org/10.1016/j.addr.2022.114531

Uzhytchak, M., Smolkova, B., Lunova, M., Frtus, A., Jirsa, M., Dejneka, A., Lunov, O. (2023) Lysosomal nanotoxicity: Impact of nanomedicines on lysosomal function, *Advanced Drug Delivery Reviews*, 197(1), pp. 1-41. https://doi.org/10.1016/j.addr.2023.114828

Valstar, M., Marchal, J., Grootenhuis, M., Colland, V., Wijburg, F. (2011) Cognitive development in patients with Mucopolysaccharidosis type III (Sanfilippo syndrome), *Orphanet Journal of Rare Diseases*, 43(6), pp. 1-6.

Walkley, S. (2004) Secondary accumulation of gangliosides in lysosomal storage disorders, *Seminars in Cell & Developmental Biology*, 15(4), pp. 433-444. https://doi.org/10.1016/j.semcdb.2004.03.002

Wang, D., Tai, P., Gao, G. (2019) Adeno-associated virus vector as a platform for gene therapy delivery, *Nature Reviews Drug Discovery*, 18(1), pp. 358-378.

Whyte, L., Hopwood, J., Hemsley, K., Lau, A. (2015) Variables influencing fluorometric *N*-sulfoglucosamine sulfohydrase (SGSH) activity measurement in brain homogenates, *Molecular Genetics and Metabolism Reports*, 5(1), pp. 60-62. https://doi.org/10.1016/j.ymgmr.2015.10.005

Winner, L., Beard, H., Hassiotis, S., Lau, A., Luck, A., Hopwood, J., Hemsley, K. (2016) A Preclinical Study Evaluating AAVrh10-Based Gene Therapy for Sanfilippo Syndrome, *Human Gene Therapy*, 27(5), pp. 363-375. https://doi.org/10.1089/hum.2015.170

Wolfenden, C., Wittowski, A. Hare, D. (2017) Symptoms of Autism Spectrum Disorder (ASD) in Individuals with Mucopolysaccaride Disease Type III (Sanfilippo Syndrome): A Systematic Review, *Journal of Autism and Developmental Disorders*, 47(1), pp. 3620-3633. https://doi.org/10.1007/s10803-017-3262-6

World Health Organisation. (2021) Global status report on the public health response to dementia, *World Health Organisation*, Geneva. <https://www.who.int/publications/i/item/9789240033245>

Zu, H., Gao, G. (2021) Non-viral Vectors in Gene Therapy: Recent Development, Challenges, and Prospects, *The AAPS Journal*, 23(78), pp. 1-12.

Appendix A: Preliminary GFP Work

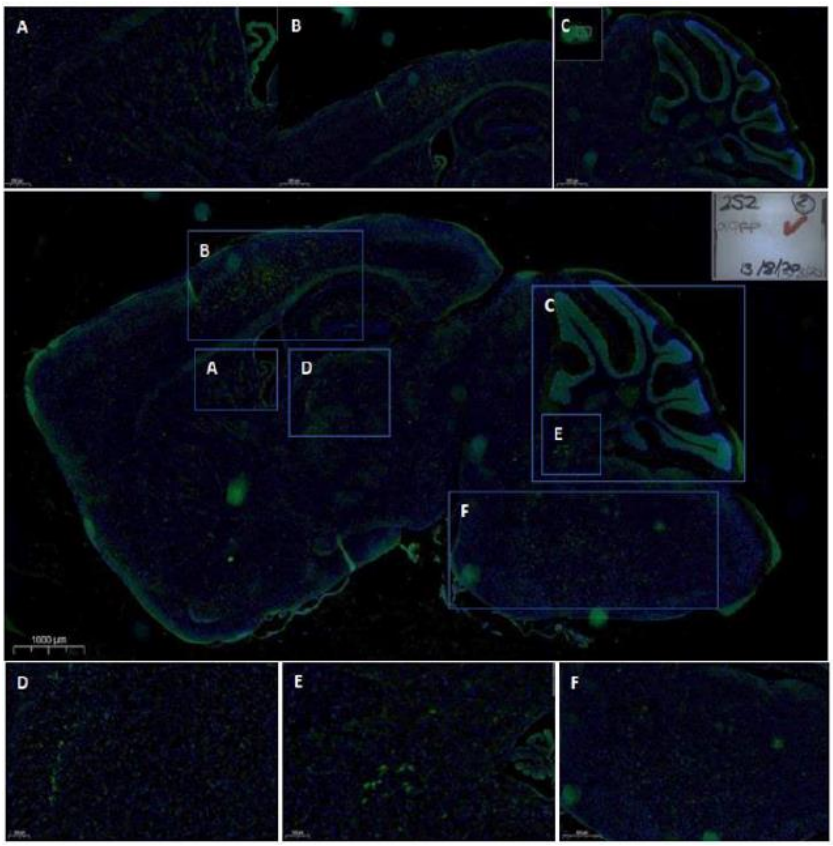

Figure A.1: *Green fluorescent protein expression throughout sagittal section of mouse brains after treatment with pDNA carrying lipid nanoparticles. Mice (n=6) received injections of* $5x10^{12}$ *plasmid copies/kg within thalamus and striatum bilaterally at 6 weeks of age, and were euthanized 4 weeks post-treatment. GFP signal visualised by histological fluorescence with regions A-F of the section also shown in greater detail. (Childhood Dementia Research Group, unpublished data).*

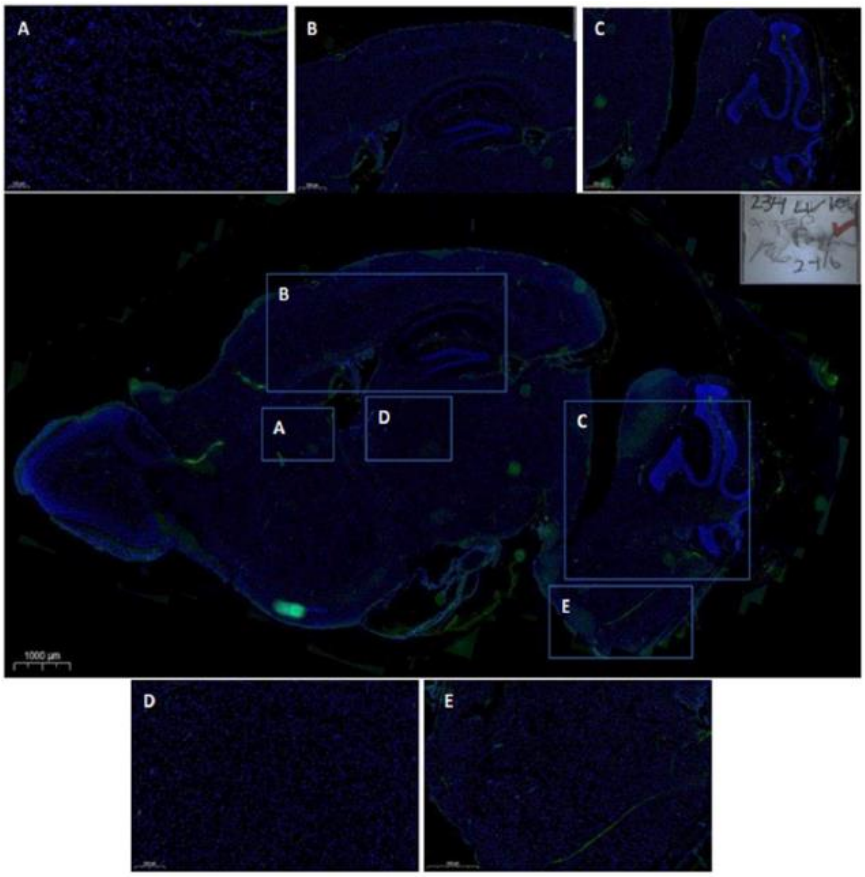

Figure A.2: *Green fluorescent protein expression throughout sagittal section of mouse brains after treatment with vehicle-only saline control. Mice (n=6) received injections within thalamus and striatum bilaterally at 6 weeks of age, and were euthanized 4 weeks post-treatment. GFP signal visualised by histological fluorescence with regions A-E of the section also shown in greater detail (Childhood Dementia Research Group, unpublished data).*

Appendix B: Preparation of Chemical Reagents, Buffers and Fixes.

B.1 Preparation of 10mM Citrate Buffer

Trisodium Citrate Dihydrate was combined with Milli-Q water at a ratio of 2.49 g/L, and pH was adjusted to 7.4 via addition of sodium hydroxide and hydrochloric acid, before autoclaving for sterility and storing at 4^{o}C.

B.2 Preparation of HEPES buffered saline

HEPES and Sodium Chloride was combined with Milli-Q water at a ratio of 4.766 and 8.473 g/L, respectively. pH was adjusted to 7.4 via addition of sodium hydroxide, before autoclaving for sterility and storing at 4^{o}C.

B.3 Preparation of Phosphate Buffered Saline for mouse and histological work

Sodium chloride, potassium chloride, di-sodium hydrogen orthophosphate, and potassium hydrogen orthophosphate are combined with Milli-Q water at a ratio of 40, 1, 5.75, and 1 g/L respectively. This produces a 10x stock.

10x PBS stock is combined with Milli-Q water at a 100 ml to 900 ml ratio to produce a 1x working stock. pH is adjusted to 7.4 via the addition of sodium hydroxide & hydrochloric acid, before autoclaving for sterility and storing at 4^{o}C.

B.5 Preparation of TE Buffer for PicoGreen DNA quantitation assay

Tris and EDTA were combined with Milli-Q water at a ratio of 0.121 and 0.0292 g/100 ml respectively.

B.6 Preparation of 4% Paraformaldehyde (PFA) for cell & tissue fixation

PBS was warmed to 50^{o}C before being slowly added to pre-measured PFA powder in a fumehood, at a ratio of 1000 ml PBS to 40g powder. The mix was heated to 60^{o}C and stirred, and pH was stabilized at 7.4 via addition of sodium hydroxide.

B.7 Preparation of Davidson's Fix for eye fixation

4-parts 37% Formalin, 3-parts glacial acetic acid, 2-parts 100% ethanol, and 1-part Milli-Q water were combined in a fumehood. The resulting solution was used within 24 hours.

B.8 Preparation of Tris-NaCl as a tissue homogenisation buffer

Tris and sodium chloride were combined with Milli-Q water at a ratio of 1.23 and 7.3 g/L respectively. pH was adjusted to 7.4 using hydrogen chloride.

B.9 Preparation of 0.2M Sodium Acetate for sample dialysis

Sodium acetate was combined with Milli-Q water at a ratio of 8.2 g/L, and pH adjusted to exactly 6.5 using glacial acetic acid.

B.10 Preparation of McIlvaine's phosphate/citrate buffer (Pi/Ci buffer)

Solution A was prepared by combining citric acid with Milli-Q water at a ratio of 4.2 g/100 ml. Solution B was prepared by combining disodium hydrogen phosphate dehydrate with Milli-Q water at a ratio of 7.1 g/100 ml.

Solution A, Solution B, and 20% sodium azide were combined in a fumehood at a ratio of 27.25 ml, 72.25 ml, and 100 µl respectively, before being stabilized to a pH of 6.7 and stored at 4^{o}C.

Attribution: Preparation of buffer stocks carried out by Dr Adeline Lau prior to project start.

B.11 Preparation of SGSH assay stop buffer (0.5 M Na_2CO_3/$NaHCO_3$)

Solution A was prepared by combining sodium carbonate with Milli-Q water at a ratio of 10.6 g/100 ml. Solution B was prepared by combining sodium bicarbonate with Milli-Q water at a ratio of 8.4 g/100 ml.

90 ml of solution A was then combined with 10 ml of solution B, along with 100 ml of Milli-Q water and 50 µl 20% Triton X-100, before being stabilized at pH 10.7 and stored at 4C.

Attribution: Preparation of buffer stocks carried out by Dr Adeline Lau prior to project start.

B.12 Preparation of 75nM Lysotracker working solution

1mM lysotracker red stock was diluted in 37^{o}C cell growth media at a ratio of 1 µl/ml to produce a 1µM dilution. That 1 µM lysotracker stock was then diluted in additional 37^{o}C cell growth media at a ratio of 15 µl/200 µl to produce a 75 nM working stock.

B.13 Preparation of 10% Trypsin-EDTA for cell culture work

Sterile 10x Trypsin-EDTA was combined with Sterile Dulbecco's PBS at a 1:9 ratio under sterile conditions and stored at 4^{o}C.

B.14 Preparation of growth media for human fibroblast cell lines

FCS, L-Glutamine, and Pen-Strep were combined in EMEM base media at a ratio of 10, 1, and 1 ml/100 ml respectively under sterile conditions. The resulting media was mixed via inversion and stored at 4^{o}C.

Appendix C: Subsequent Studies

C.1 Further work - LIMP2 histological staining of mouse brain tissue.

Lysosomal integral membrane protein type 2 (LIMP2) is a protein closely linked with lysosomal function and as such is elevated in lysosomal storage disorders such as Sanfilippo syndrome (Heybrock *at al.* 2019).

It was hypothesized that use of sensitive histological techniques would show a significant difference between the MPS-IIIA control group and the nanoparticle treatment group, correcting the latter toward the phenotype of the wildtype control group. As seen in Figure 4.1, following histological work carried out in the CDRG lab investigated several regions of the PFA-fixed half-brain samples obtained in method Section 2.4.1.3.

No significant difference was found between the wildtype and MPS-IIIA control groups, or between the MPS-IIIA control group and the nanoparticle treatment group.

Attribution: All LIMP2 histological work and analysis was carried out by Ms Helen Beard.

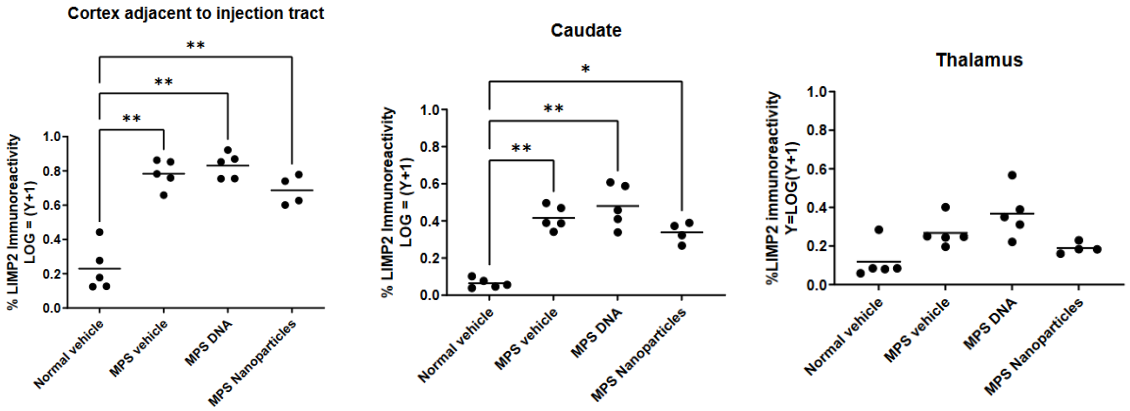

Figure 4.1: *LIMP2 Immunoreactivity of mouse half-brain samples. Mice underwent 30-days growth after intraparenchymal treatment with plasmid-carrying nanoparticles or naked DNA plasmids, both at 5x10^{12} plasmid copies per kilogram of bodyweight, along with PBS-treated vehicle controls. Data shown as mean ± SEM from 5 mouse samples per treatment, or 4 for the nanoparticle treatment group. Statistical analysis performed via one-way ANOVA with Bonferroni post-hoc testing in GraphPad Prism.*